

Shortcuts to adiabaticity for trapped ultracold gases

Jean-François Schaff¹, Pablo Capuzzi², Guillaume Labeyrie¹
and Patrizia Vignolo¹

¹ Université de Nice-Sophia Antipolis, Institut non linéaire de Nice, CNRS, 1361 route des Lucioles, F-06560 Valbonne, France

² Universidad de Buenos Aires, FCEN, Departamento de Física and Instituto de Física de Buenos Aires, CONICET, Ciudad Universitaria, Pab. I C1428EGA Buenos Aires, Argentina

E-mail: jean-francois.schaff@inln.cnrs.fr

Abstract. We study, experimentally and theoretically, the controlled transfer of harmonically trapped ultracold gases between different quantum states. In particular we experimentally demonstrate a fast decompression and displacement of both a non-interacting gas and an interacting Bose-Einstein condensate which are initially at equilibrium. The decompression parameters are engineered such that the final state is identical to that obtained after a perfectly adiabatic transformation despite the fact that the fast decompression is performed in the strongly non-adiabatic regime. During the transfer the atomic sample goes through strongly out-of-equilibrium states while the external confinement is modified until the system reaches the desired stationary state. The scheme is theoretically based on the invariants of motion and scaling equations techniques and can be generalized to decompression trajectories including an arbitrary deformation of the trap. It is also directly applicable to arbitrary initial non-equilibrium states.

PACS numbers: 67.85.-d, 37.10.-x

Introduction

In Quantum Mechanics, the evolution of a system described by a time-dependent Hamiltonian $H(t)$ is *adiabatic* when the transition probabilities between the instantaneous eigenstates of H are negligible. This happens when H is either time-independent, or when its rate of change is *slow* compared to the typical time-scales involved [1–3]. Nevertheless, thinking in terms of instantaneous eigenstates is often much easier than looking for the solutions of time-dependent problems. In the field of atomic physics, going from the semi-classical approach of atom-field interaction to the celebrated dressed state picture [4] illustrates the convenience of such adiabatic representations.

For this reason, many adiabatic schemes to prepare interesting quantum states were proposed. For instance, non-classical states [5, 6], or new strongly correlated states [7] can be prepared by adiabatic passage. Quantum adiabatic computation

has recently been demonstrated [8]. Yet adiabatic techniques are typically slow [3], while experimentalists are often constrained by finite lifetimes or coherence times of their samples. This motivated the search for fast schemes reproducing or approaching adiabatic transformations. Some methods use minimization techniques to optimize the transition to a target state [9–12], whereas others yield the exact same state that would have been reached after an adiabatic transformation [13, 14]. The latter are referred to as *shortcuts to adiabaticity*. In this article, we detail how such methods can be used on the motional degrees of freedom of ultracold gases confined in time-dependent harmonic traps, and experimentally demonstrate the validity of the approach. Two direct applications of the procedure are the fast cooling of atomic samples, and the suppression (or reduction) of any *parasitic excitations* which occur in experiments on ultracold gases when the trap geometry or the interactions are modified. Since the method is not restricted to equilibrium states it could be used in a variety of situations as discussed at the end of the paper.

The first part is theoretical and recalls how harmonically confined gases react to the variation of the trap. Both the one-dimensional non-interacting gas, and the three-dimensional Bose-Einstein condensate with repulsive contact interaction between particles are treated. In the second part, the method to realize shortcuts to adiabaticity are detailed for these two systems, and examples are given. The third part focuses on the experimental realization of these methods. Rapid decompressions have been performed on both a non-interacting gas and a Bose-Einstein condensate. The practical limitations which degrade the results are discussed. In the last part of the article, we attempt to generalize the problem to an arbitrary variation of the three-dimensional harmonic potential and give other examples of shortcuts which may be of experimental relevance.

1. Scaling properties of harmonically confined ultracold gases: two examples

In this section, we recall how the density and velocity distributions of a one-dimensional (1D) non-interacting gas are affected by a change of the harmonic confinement. In 1D, the harmonic trap is fully described by its time-dependent angular frequency $\omega(t)$, and minimum position $q_0(t)$. We show that the dynamics is fully described by two scaling functions, one associated to the cloud's size, the other to its centre-of-mass position, and exhibit the exact solutions of the Schrödinger equation. This will be used in the rest of the paper to realize shortcuts to adiabaticity (cf. Sec. 2). Similar scaling properties are also recalled for Bose-Einstein condensates (BECs) with strong interactions in the Thomas-Fermi regime. The analogy between the invariant method used for the non-interacting gas [15], and the scaling often used for BECs [16–18] is underlined.

1.1. The non-interacting gas

We consider a 1D non-interacting gas confined in the most general time-dependent harmonic potential, described by the one particle Hamiltonian

$$H(q, p, t) = \frac{p^2}{2m} + \frac{1}{2}m\omega^2(t)[q - q_0(t)]^2, \quad (1)$$

where q and p are conjugate variables, and m is the mass of a particle. We first recall how dynamical invariants can be used to find the general solutions of the Schrödinger equation.

1.1.1. Definition and properties of dynamical invariants In 1969 Lewis and Riesenfeld [15] generalized the concept of invariant of motion to the case of explicitly time-dependent Hamiltonians $H(q, p, t)$. Such Lewis invariants (also called dynamical invariants, or first integrals) can be used to solve the Schrödinger equation

$$i\hbar\frac{\partial|t\rangle}{\partial t} = H(q, p, t)|t\rangle. \quad (2)$$

Given a time-dependent Hamiltonian $H(q, p, t)$, a time-dependent hermitian operator $I(q, p, t)$ is a dynamical invariant of the system described by H if it is constant under Hamiltonian evolution, that is if

$$\frac{dI}{dt} \equiv \frac{\partial I}{\partial t} + \frac{1}{i\hbar}[I, H] = 0. \quad (3)$$

In this case, the following properties hold [15]:

- (i) if $|t\rangle$ is a solution of (2), then $I|t\rangle$ is also a solution of (2),
- (ii) the eigenvalues $\lambda(t)$ and associated eigenvectors $|\lambda; t\rangle$ of I are *a priori* time-dependent. We assume they form a complete set. It turns out that the eigenvalues are actually constant: $\lambda(t) = \lambda$. They are real because I is hermitian.
- (iii) The eigenvectors of I satisfy

$$\text{for all } \lambda, \lambda' \text{ such that } \lambda \neq \lambda', \quad \langle \lambda'; t | i\hbar\frac{\partial}{\partial t} | \lambda; t \rangle = \langle \lambda'; t | H | \lambda; t \rangle. \quad (4)$$

- (iv) If we assume that I does not contain the operator $\partial/\partial t$, then the set of vectors $\{e^{i\alpha_\lambda(t)}|\lambda; t\rangle, \alpha_\lambda(t) \in \mathbb{R}(t)\}$ is also a complete set of eigenvectors of I . If these functions are chosen to solve the equations

$$\frac{d\alpha_\lambda}{dt} = \langle \lambda; t | i\frac{\partial}{\partial t} - \frac{H}{\hbar} | \lambda; t \rangle \quad (5)$$

then Eq. (4) also holds for $\lambda' = \lambda$. Using the fact that the set is complete, this gives the general solutions of the time-dependent Schrödinger equation as

$$|t\rangle = \sum_{\lambda} c_{\lambda} e^{i\alpha_{\lambda}(t)} |\lambda; t\rangle, \quad (6)$$

where the c_{λ} 's are constant complex numbers.

The solutions of the Schrödinger equation are thus given by the knowledge of an invariant $I(q, p, t)$, any set of its time-dependent eigenvectors, and the phases $\alpha_\lambda(t)$ which must solve Eqs. (5).

1.1.2. Derivation of a dynamical invariant In this section, we give a simple derivation of the invariants of a 1D time-dependent harmonic oscillator (HO) described by (1). We use the classical formalism to derive the invariant, which is also an invariant of the corresponding quantum system.

The canonical equations of motion associated with the Hamiltonian (1) are

$$\frac{dq}{dt} = \{q, H\} = \frac{p}{m}, \quad (7a)$$

$$\frac{dp}{dt} = \{p, H\} = -m\omega^2(t)[q - q_0(t)], \quad (7b)$$

where $\{A, B\} \equiv \frac{\partial A}{\partial q} \frac{\partial B}{\partial p} - \frac{\partial A}{\partial p} \frac{\partial B}{\partial q}$ are the Poisson brackets of two observables A and B .

When the angular frequency $\omega(t)$ and trap centre $q_0(t)$ vary, one expects the cloud to be displaced and to change its size, thus one can introduce a canonical change of variables

$$Q = \frac{q - q_{\text{cm}}(t)}{b(t)}, \quad P = P(q, p, t), \quad \tau = \tau(t), \quad (8)$$

leading to a new Hamiltonian H' . One has to derive conditions on the real dimensionless function b , and the displacement function q_{cm} such that the transformation is canonical. For this, we look for a new Hamiltonian of the form

$$H' = \frac{P^2}{2m} + \frac{1}{2}m\omega_0^2 Q^2 + f(\tau), \quad (9)$$

where ω_0 is a constant angular frequency. The Hamiltonian explicitly depends on time only through the function $f(\tau)$ (which does not contain the variables Q and P). The transformation (8) is canonical if

$$\frac{dQ}{d\tau} = \{Q, H'\}, \quad (10a)$$

$$\frac{dP}{d\tau} = \{P, H'\}. \quad (10b)$$

From Eq. (10a) one deduces that

$$d\tau = b^{-2} dt \quad (11)$$

and that

$$P = b(p - m\dot{q}_{\text{cm}}) - m\dot{b}(q - q_{\text{cm}}), \quad (12)$$

where $\dot{}$ denotes the derivation with respect to time t . From Eq. (10b), one finds the functions b and q_{cm} must obey the two differential equations

$$\ddot{b} + \omega^2(t)b = \frac{\omega_0^2}{b^3}, \quad (13)$$

$$\ddot{q}_{\text{cm}} + \omega^2(t)[q_{\text{cm}}(t) - q_0(t)] = 0. \quad (14)$$

When these two equations are satisfied, the quantity

$$I = \frac{P^2}{2m} + \frac{1}{2}m\omega_0^2 Q^2 \quad (15)$$

which appears in the new Hamiltonian is a Lewis invariant. This can be proved directly by checking that Eq. (3) is verified.

The choice of the function $f(\tau)$ in H' is irrelevant for the dynamics, since doing the change of Hamiltonian

$$H' \rightarrow H' - f(\tau) = I \quad (16)$$

corresponds to a gauge transformation which changes the phase of the wave function in the following manner:

$$\psi_{H'}(Q, \tau) \rightarrow \psi_I(Q, \tau) = e^{\frac{i}{\hbar}F(\tau)}\psi_{H'}(Q, \tau), \quad (17)$$

where F is a primitive of f .

1.1.3. Wave functions Once an invariant has been found, the results of section 1.1.1 can be used to calculate the wave functions of the time-dependent HO (1). We use Dirac's method to calculate the wave function of the time-independent HO (15). We define dimensionless variables

$$\xi = \sqrt{\frac{m\omega_0}{\hbar}}Q, \quad \pi = \frac{1}{\sqrt{m\hbar\omega_0}}P, \quad (18)$$

satisfying the commutation relation $[\xi, \pi] = i$, and introduce the lowering and raising operators

$$a = \frac{1}{\sqrt{2}}(\xi + i\pi), \quad a^\dagger = \frac{1}{\sqrt{2}}(\xi - i\pi). \quad (19)$$

The invariant reads

$$I = \hbar\omega_0(a^\dagger a + 1/2). \quad (20)$$

The eigenstates $|n\rangle$ of the number operator $\hat{n} \equiv a^\dagger a$ are the eigenstates of I and satisfy

$$a|n\rangle = \sqrt{n}|n-1\rangle, \quad a^\dagger|n\rangle = \sqrt{n+1}|n+1\rangle, \quad n \in \mathbb{N}. \quad (21)$$

The eigenvalues of I are

$$\lambda_n = \left(n + \frac{1}{2}\right)\hbar\omega_0, \quad n \in \mathbb{N}. \quad (22)$$

The wave function $\psi_0(q, t) \equiv \langle q|0\rangle$ is calculated by solving the equation

$$a|0\rangle = 0 \quad (23)$$

in $|q\rangle$ representation. The expression of π is obtained from $p = -i\hbar\partial/\partial q$, and Eqs. (18) and (8), and reads

$$\pi = -i\frac{\partial}{\partial \xi} - \frac{b\dot{b}}{\omega_0}\xi - \sqrt{\frac{m}{\hbar\omega_0}}b\dot{q}_{\text{cm}}. \quad (24)$$

Imposing the normalization condition $\int dq |\psi_0(q, t)|^2 = 1$, and calculating the time-dependent phase corresponding to the initial Hamiltonian (1), we obtain the wave function

$$\psi_0(q, t) = \frac{\pi^{-1/4}}{\sqrt{a_{\text{ho}}b}} \exp \left[-\frac{1}{2} \left(\frac{q - q_{\text{cm}}}{a_{\text{ho}}b} \right)^2 \right] e^{-\frac{i}{\hbar} F(t)} e^{i\phi(q, t)} e^{-\frac{i}{\hbar} \lambda_0 \int_0^t dt' / b^2} \quad (25)$$

where

$$\phi(q, t) = \frac{m}{\hbar} \left[\frac{\dot{b}}{2b} q^2 + \frac{1}{b} (\dot{q}_{\text{cm}} b - q_{\text{cm}} \dot{b}) q \right], \quad (26)$$

$$F(t) = \frac{m}{2} \int_0^t dt' \left[\frac{1}{b^2} (\dot{q}_{\text{cm}} b - q_{\text{cm}} \dot{b})^2 - \omega_0^2 \frac{q_{\text{cm}}^2}{b^4} + \omega^2(t') q_0^2 \right], \quad (27)$$

and q_0 , b , q_{cm} , and their derivatives are functions of t (t' when they are under an integral symbol) and are linked by Eqs. (13) and (14). $a_{\text{ho}} = \sqrt{\hbar/m\omega_0}$ is the HO length of I .

From this expression, we see the physical meaning of the two scaling functions: $q_{\text{cm}}(t)$ is the centre of the wave function (centre of mass of a cloud which was initially at equilibrium), and $a_{\text{ho}}b$ is the width of the wave function.

The wave function associated to the eigenvalue λ_n of I is expressed in terms of the n th Hermite polynomial H_n as

$$\psi_n(q, t) = \frac{1}{2^n n!} \psi_0(q, t) H_n \left(\frac{q - q_{\text{cm}}}{a_{\text{ho}}b} \right) e^{-\frac{i}{\hbar} (\lambda_n - \lambda_0) \int_0^t dt' / b^2}. \quad (28)$$

1.2. The case of an interacting Bose-Einstein condensate

For the corresponding three-dimensional (3D) interacting system of N particles, the Hamiltonian is

$$H = \sum_{i=1}^N \left[\frac{\mathbf{p}_i^2}{2m} + U(\mathbf{r}_i, t) \right] + \sum_{i < j} V(\mathbf{r}_j - \mathbf{r}_i). \quad (29)$$

The potential U is supposed to be a time-dependent 3D HO, and the rotation of this harmonic confinement is excluded for the moment (the trap keeps the same eigenaxes):

$$U(\mathbf{r}, t) = \frac{1}{2} m \left\{ \omega_x^2(t) [r_x - r_x^0(t)]^2 + \omega_y^2(t) [r_y - r_y^0(t)]^2 + \omega_z^2(t) [r_z - r_z^0(t)]^2 \right\}, \quad (30)$$

V is the interaction potential between two particles, which is well approximated by a delta function for ultracold gases [19].

The procedure described in Sec. 1.1 cannot be easily adapted, because it would require the knowledge of an invariant of this many-body system. But, when dealing with a BEC, the dynamics is well described by a single particles wave function, whose evolution obeys a non-linear Schrödinger equation, the Gross-Pitaevskii equation (GPE) [19].

1.2.1. *Scaling approach* Let us consider a quantum system described by the wave function $\psi(\mathbf{r}, t)$, whose time evolution is given by the GPE

$$i\hbar \frac{\partial}{\partial t} \psi(\mathbf{r}, t) = \left[-\frac{\hbar^2}{2m} \Delta + U(\mathbf{r}, t) + \tilde{V} N |\psi(\mathbf{r}, t)|^2 \right] \psi(\mathbf{r}, t), \quad (31)$$

with m , the mass of the particles, N the number of particles, and $\tilde{V} = 4\pi\hbar^2 a_s/m$ the interaction coupling constant generated by s -wave scattering between particles, characterized by the scattering length a_s . Analogously to the non-interacting case, we wish to write the solution of the time-dependent GPE as a function of the solution of a time-independent one expressed in a suitable frame of reference. Following this line, a strategy to solve Eq. (31) is to find a change of variables $\boldsymbol{\rho}(\mathbf{r}, \{b_i(t)\}, \{r_i^{\text{cm}}(t)\})$ where the b_i 's and the r_i^{cm} 's are scaling and translation functions such that Eq. (31) can be written as a time-independent equation (i.e. a GPE with a *time-independent* potential) on the wave function $\chi(\boldsymbol{\rho}, \tau)$, defined by the relation

$$\psi(\mathbf{r}, t) = \mathcal{A}(t) \chi(\boldsymbol{\rho}, \tau) e^{i\phi(\mathbf{r}, t)}, \quad (32)$$

$\mathcal{A}(t)$ being a time-dependent normalization factor and $\phi(\mathbf{r}, t)$ a space- and time-dependent phase. All the dynamics induced by the time-dependent potential is *transferred* to the functions $\{b_i(t)\}$ and $\{r_i^{\text{cm}}(t)\}$, and the differential equations they have to satisfy (similar to Eqs. (13) and (14)). If one can solve the new time-independent equation on χ , one solves Eq. (31) and knows the wave function $\psi(\mathbf{r}, t)$.

Equation (31) is invariant under the transformation

$$\forall i \in \{x, y, z\}, \quad \rho_i = \frac{r_i - r_i^{\text{cm}}(t)}{b_i(t)} \quad (33)$$

in any of the following cases:

- (i) in the non-interacting limit [16, 20]: in this case the system is equivalent to three independent HO of the kind treated in Sec. 1.1,
- (ii) for a suitable driving of the interaction term \tilde{V} [20], that is, assuming one can control $\tilde{V}(t)$ at will (for cold gases, this can be done using Feshbach resonances),
- (iii) in the TF limit [17].

This third case, which is detailed in the following section, is used in the rest of the paper.

1.2.2. *Condensate wave function in the Thomas-Fermi approximation* Given a time-dependent Gross-Pitaevskii equation, the TF approximation consists in neglecting the kinetic-energy-like term in the $\boldsymbol{\rho}$ -frame of reference, i.e. $-\hbar^2/(2m) \sum_i b_i^{-2} \partial^2 \chi / \partial \rho_i^2$, supposed to be small compared to the interaction term [17, 18]. In this regime, provided that $\mathcal{A}(t) = (\prod_i b_i)^{-1/2}$ and that

$$\phi(\mathbf{r}, t) = \frac{m}{\hbar} \left\{ \sum_i \left[\frac{r_i^2 \dot{b}_i}{2 b_i} + \frac{r_i}{b_i} (\dot{r}_i^{\text{cm}} b_i - r_i^{\text{cm}} \dot{b}_i) \right] \right\} + \phi_0(t), \quad (34)$$

with

$$\phi_0(t) = -\frac{m}{2\hbar} \sum_i \int_0^t dt' \left\{ \frac{1}{b_i^2} \left(\dot{r}_i^{\text{cm}} b_i - r_i^{\text{cm}} \dot{b}_i \right)^2 - \omega_i^2(0) \frac{(r_i^{\text{cm}})^2}{b_i^4} + [\omega_i(t') r_i^0(t')]^2 \right\} \quad (35)$$

where the scaling and translation functions are solutions of

$$\forall i \in \{x, y, z\}, \quad \ddot{b}_i + \omega_i^2(t) b_i = \frac{\omega_i^2(0)}{b_i b_x b_y b_z}, \quad (36)$$

$$\ddot{r}_i^{\text{cm}} + \omega_i^2(t) [r_i^{\text{cm}} - r_i^0(t)] = 0, \quad (37)$$

one gets the following equation on χ :

$$i\hbar \frac{\partial}{\partial \tau} \chi(\boldsymbol{\rho}, \tau) = \left[U(\boldsymbol{\rho}, 0) + \tilde{V} N |\chi(\boldsymbol{\rho}, \tau)|^2 \right] \chi(\boldsymbol{\rho}, \tau), \quad (38)$$

where we defined a rescaled time

$$\tau(t) = \int_0^t \frac{dt'}{\Pi_i b_i(t')}. \quad (39)$$

If at $t = 0$ the condensate is at equilibrium, the solution of Eq. (38) is

$$\chi(\boldsymbol{\rho}, \tau) = \left[\frac{\mu - U(\boldsymbol{\rho}, 0)}{\tilde{V} N} \right]^{1/2} e^{-i\frac{\mu}{\hbar}\tau}, \quad (40)$$

μ being the chemical potential. This gives the typical inverted parabola density profile whose sizes evolve in time as $R_i(t) = R_i(0) b_i(t)$, $R_i(0) = \sqrt{2\mu_0/m\omega_i^2(0)}$ being the initial TF radii.

2. Shortcuts to adiabaticity

In this section the definition of a shortcut to adiabaticity is given, and the results of Sec. 1 are used to derive angular frequency trajectories realizing such shortcuts, for both non-interacting gases and interacting BECs confined in time-dependent harmonic traps.

2.1. Shortcut to adiabaticity based on an invariant of motion

For a system described by a Hamiltonian $H(t)$, a *shortcut to adiabaticity* is realized when another Hamiltonian $H'(t)$ can be found, such that the state obtained after a finite time of evolution with $H'(t)$ is *identical* (up to a global phase factor) to the final state of the adiabatic evolution with $H(t)$. Shortcuts to adiabaticity are *not* adiabatic; only the final state is identical to that obtained after an adiabatic evolution.

The possibility of such shortcuts has been known for a long time. For instance, in the case of a HO with a time-dependent frequency $\omega(t)$ treated in Ref. [15], when discussing the transition probability P_{sm} between two instantaneous eigenstates $|s; t\rangle$

and $|m; t\rangle$, the authors noticed that some trajectories $\omega(t)$ could lead to the same result as the adiabatic case, namely

$$P_{sm} = \delta_{sm}. \quad (41)$$

Such shortcuts to adiabaticity can thus be realized simply by engineering the time-dependent parameters of the Hamiltonian.

A practical method to find a class of appropriate $\omega(t)$ was detailed by Chen et al. [14]. In this case, the Hamiltonian is chosen to be time-independent (but with different frequencies) outside the time interval $t \in [0, t_f]$. An invariant is engineered to commute with the Hamiltonian outside this interval. This yields a specific $\omega(t)$ for which all the eigenstates of $H(t < 0)$ are exactly mapped to the corresponding ones of $H(t > t_f)$ after the evolution for $t \in [0, t_f]$. Up to a global phase and a rescaling of energies and lengths, the final state (at time $t = t_f$) is identical to the initial one ($t = 0$), i.e. if the initial state was

$$|\psi; t \leq 0\rangle = \sum_n c_n |n; t = 0\rangle e^{-i\omega_n(0)t}, \quad (42)$$

where $\{|n; t\rangle, n \in \mathbb{N}\}$ is a basis of instantaneous eigenstates of $H(t)$ and $\{\hbar\omega_n(t)\}$ the corresponding eigenvalues, and $\sum_n |c_n|^2 = 1$, then the final state is

$$|\psi; t \geq t_f\rangle = e^{i\Phi} \sum_n c_n |n; t_f\rangle e^{-i\omega_n(t_f)t}. \quad (43)$$

This is true even if the initial state is not an equilibrium state.

2.1.1. Frequency trajectory for a non-interacting gas The Hamiltonian is assumed to have the form

$$H = \frac{p^2}{2m} + \frac{1}{2}m\omega^2(t)q^2 + mgq, \quad (44)$$

which is identical to (1), with the additional constraint $q_0(t) = -g/\omega^2(t)$ (and a gauge transformation consisting in adding $-m\omega^2(t)q_0^2(t)/2$ to H). It describes a single particle in a harmonic trap subject to a constant force, which, in the experiments presented in Sec. 3, comes from gravity. The angular frequency $\omega(t)$ is assumed to be constant outside the interval $t \in [0, t_f]$. During this interval, the problem is to find the appropriate frequency trajectory $\omega(t)$, connecting the initial trap of initial frequency $\omega(0)$ to a final trap of frequency $\omega(t_f)$, for the decompression (or compression if $\omega(0) < \omega(t_f)$) to implement a shortcut to adiabaticity. Figure 1 shows the initial and final situations assuming a decompression ($\omega(t_f) < \omega(0)$).

We used the strategy introduced by Chen et al. [14]. If the invariant commutes with the Hamiltonian

$$[I, H] = 0 \quad (45)$$

for $t \leq 0$ and $t \geq t_f$, and provided that the functions b and q_{cm} are sufficiently continuous, the stationary states of $H(t \leq 0)$ will be transferred to the corresponding ones of $H(t \geq t_f)$.

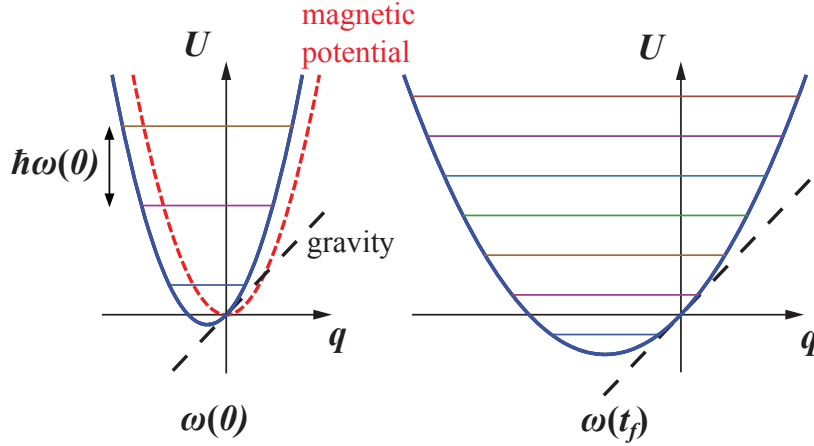


Figure 1. Schematic representation of the trap decompression. The potential (plain blue line) is the sum of the gravitational potential (dashed black line) and the harmonic magnetic potential (dashed red line). When the trap frequency is changed from $\omega(0)$ to $\omega(t_f)$, the lengths are multiplied by $\gamma = \sqrt{\omega(0)/\omega(t_f)}$, and the energies divided by γ^2 . Because of gravity, the trap centre shifts vertically by $\Delta q = -g [1/\omega^2(t_f) - 1/\omega^2(0)]$.

It is convenient to use the dimensionless function

$$c(t) = -\frac{\omega_0^2 q_{\text{cm}}(t)}{g b(t)} \quad (46)$$

instead of q_{cm} , and to rewrite Eq. (14) using the rescaled time τ (Eq. (11)). Equation (14) becomes

$$d^2c/d\tau^2 + \omega_0^2 c = \omega_0^2 b^3. \quad (47)$$

If one chooses to set $\omega_0 = \omega(0)$, and the conditions

$$b(0) = 1, \quad \dot{b}(0) = 0, \quad (48a)$$

$$c(0) = 1, \quad \dot{c}(0) = 0, \quad (48b)$$

then $I(0) = H(t \leq 0)$, and if

$$b(t_f) = \gamma, \quad \dot{b}(t_f) = 0, \quad (48c)$$

$$c(t_f) = \gamma^3, \quad \dot{c}(t_f) = 0, \quad (48d)$$

where $\gamma \equiv \sqrt{\omega_0/\omega_f}$, then $I(t_f) = \gamma^2 H(t \geq t_f) + h(t)$, where h is a function of time only. These boundary conditions thus fulfil the condition (45). Since the functions b and c must be solutions of Eqs. (13) and (47), four additional boundary conditions must be satisfied:

$$\ddot{b}(0) = 0, \quad \ddot{b}(t_f) = 0, \quad (48e)$$

$$\ddot{c}(0) = 0, \quad \ddot{c}(t_f) = 0. \quad (48f)$$

In order to construct the functions b and c satisfying these boundary conditions and the two differential equations (13) and (47), it is convenient to write all the boundary conditions on the function c and its derivatives with respect to the rescaled time τ . Using Eqs. (11) and (13), and differentiating Eq. (47) twice with respect to τ , one finds the ten conditions

$$c(0) = 1, \quad (49a)$$

$$c(\tau_f) = \gamma^3, \quad (49b)$$

and, for all $k \in \{1, 2, 3, 4\}$,

$$\frac{d^k c}{d\tau^k}(0) = 0, \quad (49c)$$

$$\frac{d^k c}{d\tau^k}(\tau_f) = 0, \quad (49d)$$

which are sufficient for the twelve boundary conditions (48). τ_f is the rescaled time corresponding to t_f : $\tau_f = \int_0^{t_f} b^{-2}(t') dt'$.

Under this form, the boundary conditions are well suited to use a polynomial ansatz for $c(\tau)$, deduce $b(\tau)$ with Eq. (47), compute $\tau(t)$ by numerically integrating Eq. (11), and obtain $b(t)$. The final step consists in using Eq. (13) to obtain the time-dependent trap frequency as $\omega^2(t) = \omega_0^2/b^4 - \ddot{b}/b$.

An example of this procedure is given on Fig. 2 for particular values of the initial and final frequencies. The final rescaled time τ_f can be chosen at will, it can be arbitrarily small, but one important constraint on the function c is that it must not lead to vanishing values of b which give infinite $\omega^2(t)$. Additional constraints on c arise from experimental requirements, such as positive $\omega^2(t)$ (attractive potentials), maximal and minimal frequencies attainable with a given setup, *speed* at which $\omega(t)$ can be varied etc. Since all this depends on a particular experimental setup, no mathematical analysis of the *best* ansatz to use was done.

For the experiments presented in Sec. 3 and in Refs. [21, 22], a polynomial of order fifteen was used:

$$c(\tau) = \sum_{k=0}^{15} c_k \left(\frac{\tau}{\tau_f} \right)^k. \quad (50)$$

The first coefficient is fixed to 1 by Eq. (49a) and c_1, \dots, c_4 are fixed to 0 by Eqs. (49c). We arbitrarily impose $c_5 = c_6 = \dots = c_{10} = 0$, which leaves five coefficients which are uniquely determined by the remaining boundary conditions (49b) and (49d). The calculation of these remaining coefficient is done by inverting the linear system corresponding to these five equations.

In principle, since there are ten BCs, a 9th order polynomial can be used, which yields a unique solution for the ten coefficients of c . Nevertheless, the obtained trajectory was not well behaved enough to be realized experimentally (the frequency was decreasing too fast in the beginning compared to what could be achieved by the apparatus). This

is the reason why a higher order polynomial was used and six coefficients were fixed to 0.

Since the polynomial can be of any order greater than 9, and the boundary conditions only impose a linear relation between nine of its coefficients, there is obviously an infinity of different solutions connecting two given initial and final states. Moreover, other functions than polynomials could be used for c , as long as they provide enough free parameters.

The obtained nonzero coefficients of (50) are given in table 1.

Table 1. Nonzero coefficients of the polynomial ansatz for $c(\tau)$ calculated from the boundary conditions (49).

c_0	c_{11}	c_{12}	c_{13}	c_{14}	c_{15}
1	$1365(\gamma^3 - 1)$	$5005(\gamma^3 - 1)$	$6930(\gamma^3 - 1)$	$4290(\gamma^3 - 1)$	$1001(\gamma^3 - 1)$

2.1.2. Example In this section we determine the trajectory used in Sec. 3.2 and in Ref. [21]. The parameters are given in table 2. Figure 2 shows the functions $c(\tau)$, $b(\tau)$, $t(\tau)$ and $\omega(t)/2\pi$ corresponding to this decompression.

Table 2. Parameters of the 1D decompression of a non-interacting thermal gas.

Initial frequency $\omega(0)/2\pi$	235.8 Hz
Final frequency $\omega(t_f)/2\pi$	15.67 Hz
Final rescaled time τ_f	5.65 ms
Corresponding duration t_f	35.0 ms

Since the exact wave functions are known, all the properties of the atomic cloud can be calculated during decompression. For instance, Fig. 3 displays the size and centre-of-mass position of a cloud initially at equilibrium in the compressed trap. These are compared to the same values if the decompression were done very slowly as in the adiabatic theorem. The clear difference between the plain and dashed curves illustrates the fact that the decompression is not adiabatic.

2.2. Shortcut to adiabaticity for an interacting Bose-Einstein condensate in the Thomas-Fermi limit

Let us suppose that $\psi(\mathbf{r}, t \leq 0)$ is a stationary state of Eq. (31). We can engineer the parameters of the potential $U(\mathbf{r}, t)$ such that $\psi(\mathbf{r}, t_f)$ is also a stationary state for $t \geq t_f$. This implies that $\chi(\rho, \tau \geq \tau_f)$, with $\tau_f = \tau(t_f)$, must be a stationary state of Eq. (38) and that $\nabla_{\mathbf{r}}\phi(\mathbf{r}, t_f) = 0$. If these two conditions hold, $\psi(\mathbf{r}, t)$ can evolve during the time interval $[0, t_f]$ between two stationary states even being strongly different from the *adiabatic stationary state* during the evolution for $0 < t < t_f$. In our experiment, the time-dependent trapping potential has a cylindrical symmetry of the form

$$U(\mathbf{r}, t) = \frac{1}{2}m\omega_{\perp}^2(t)(r_x^2 + r_z^2) + \frac{1}{2}m\omega_{\parallel}^2(t)r_y^2 + mgr_z, \quad (51)$$

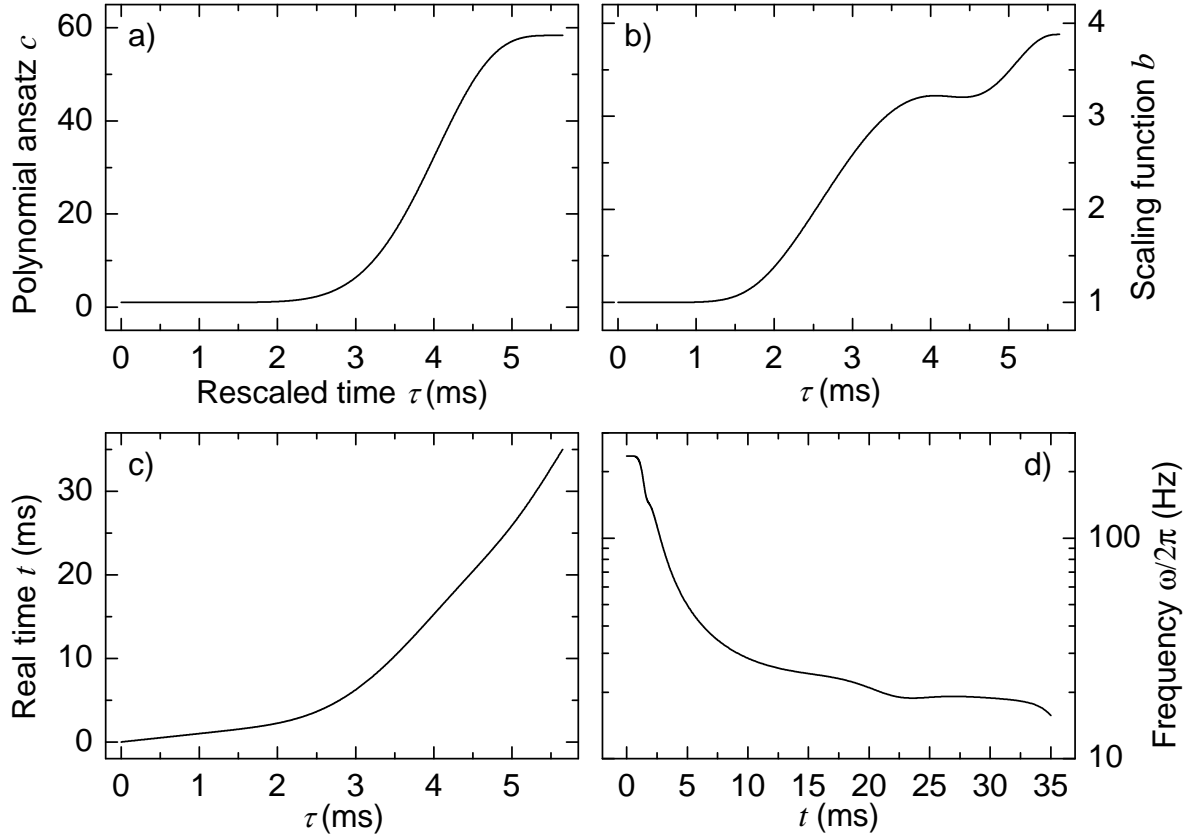


Figure 2. Determination of the frequency trajectory when the trap is decompressed from $\omega(t=0)/2\pi = 235.8$ Hz to $\omega(t_f)/2\pi = 15.67$ Hz within 35 ms (cf. parameters of Tab. 2). (a) A fifteenth order polynomial ansatz is used for the displacement function $c(\tau)$, which gives (b) the scaling function $b(\tau)$ through Eq. (47); (c) real time $t(\tau)$ is calculated by numerically integrating Eq. (11); (d) Eq. (13) is used to determine the time-dependent frequency $\omega(t)/2\pi$ (notice the logarithmic scale).

with initial and final angular frequencies $\omega_{\perp,\parallel}(0)$ and $\omega_{\perp,\parallel}(t_f) = \omega_{\perp,\parallel}(0)/\gamma_{\perp,\parallel}^2$, respectively. This case corresponds to fix $\forall t$, $r_{x,y}^0(t) = 0$ in Eq. (30) and $r_z^0(t) = -g/\omega_{\perp}^2(t)$. By introducing the dimensionless function

$$c(t) = -\frac{\omega_{\perp}^2(0) r_z^{\text{cm}}(t)}{g b_{\perp}(t)} \quad (52)$$

the differential equations (36) and (37) take the form

$$\ddot{b}_{\perp}(t) + b_{\perp}(t)\omega_{\perp}^2(t) = \omega_{\perp}^2(0)/[b_{\perp}^3(t)b_{\parallel}(t)] \quad (53)$$

$$\ddot{b}_{\parallel}(t) + b_{\parallel}(t)\omega_{\parallel}^2(t) = \omega_{\parallel}^2(0)/[b_{\parallel}^2(t)b_{\perp}^2(t)] \quad (54)$$

$$b_{\perp}^4(t)b_{\parallel}(t)\ddot{c}(t) + 2b_{\perp}^3(t)b_{\parallel}(t)\dot{b}_{\perp}(t)\dot{c}(t) + \omega_{\perp}^2(0)c(t) - \omega_{\perp}^2(0)b_{\perp}^3(t)b_{\parallel}(t) = 0. \quad (55)$$

The final state is an equilibrium state if the final TF radii verify that $R_{\perp,\parallel}(t_f)/R_{\perp,\parallel}(0) = \gamma_{\perp,\parallel}^2$, if the vertical centre-of-mass position fulfils the condition $r_z^{\text{cm}}(t_f)/r_z^{\text{cm}}(0) = \gamma_{\perp}^4$, and if the condensate flow is null, namely if $\nabla\phi = 0$. These

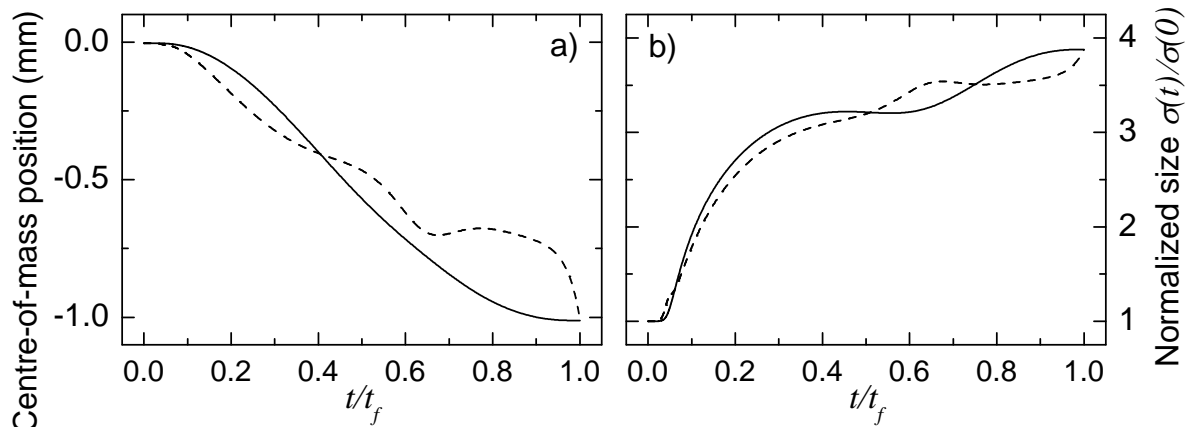


Figure 3. Expected (a) centre-of-mass position and (b) cloud size during a fast decompression (same parameters as Tab. 2 and Fig. 2). The dashed curves correspond to the same values in the adiabatic limit $t_f \rightarrow \infty$. The adiabatic centre-of-mass position is the trap minimum $q_{\text{ad.}}(t) = -g/\omega^2(t)$, and the adiabatic size is $\sigma_{\text{ad.}}(t) = \sqrt{\omega_0/\omega(t)}\sigma(0)$.

lead to the boundary conditions $\dot{c}(0) = \dot{c}(t_f) = \dot{b}_{\perp,\parallel}(0) = \dot{b}_{\perp,\parallel}(t_f) = 0$ and $c(0) = 1$, $c(t_f) = \gamma_{\perp}^{14/5}\gamma_{\parallel}^{2/5}$, $b_{\perp,\parallel}(0) = 1$, $b_{\perp}(t_f) = \gamma_{\perp}^{6/5}\gamma_{\parallel}^{-2/5}$ and $b_{\parallel}(t_f) = \gamma_{\perp}^{-4/5}\gamma_{\parallel}^{8/5}$. These latter imply that $\ddot{b}_{\perp,\parallel}(0) = \ddot{b}_{\perp,\parallel}(t_f) = 0$ must hold as well, giving sixteen independent boundary conditions (BC).

Our procedure to engineer $\omega_{\perp,\parallel}(t)$ is to reduce the dimensionality of the problem by only considering the trajectories that lead to a constant axial size. This corresponds to keeping $b_{\parallel}(t) = b_{\parallel}(0)$ for any t , fixing a trap decompression with $\gamma_{\perp} = \gamma_{\parallel}^2$. In this case, Eqs. (53)-(55) reduce to

$$\ddot{b}_{\perp}(t) + b_{\perp}(t)\omega_{\perp}^2(t) = \omega_{\perp}^2(0)/b_{\perp}^3(t) \quad (56)$$

$$\omega_{\parallel}(t) = \omega_{\parallel}(0)/b_{\perp}(t) \quad (57)$$

$$b_{\perp}^4(t)\ddot{c}(t) + 2b_{\perp}^3(t)\dot{b}_{\perp}(t)\dot{c}(t) + \omega_{\perp}^2(0)c(t) - \omega_{\perp}^2(0)b_{\perp}^3(t) = 0. \quad (58)$$

Equation (56) is identical to Eq. (13) and Eq. (58) is nothing but Eq. (47) expressed with the real time (the rescaled time being given by Eq. (39) instead of Eq. (11)). Thus we can exploit for $b_{\perp}(t)$ and $c(t)$ the solutions obtained for the non-interacting gas, provided that the axial frequency is varied according to Eq. (57).

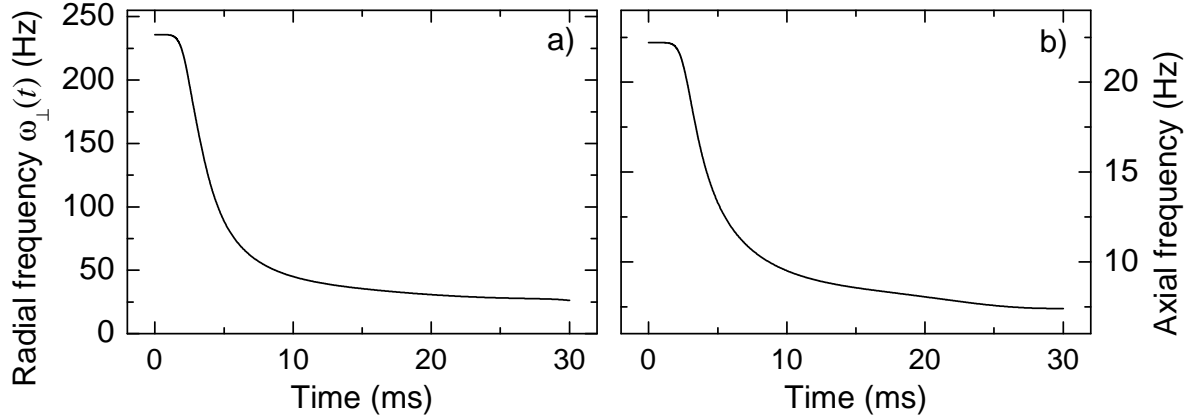
2.2.1. Example As an example of the procedure described above, we determine the trajectories used in Sec. 3.3 and in Ref. [22]. The decompression parameters are given in table 3. The radial frequency is reduced by a factor of 9, and the axial frequency by a factor of 3.

The obtained trajectories are represented in Fig. 4.

2.2.2. Validity of the Thomas-Fermi approximation To check the validity of the Thomas-Fermi approximation that led to the trajectories of Fig. 4, three-dimensional

Table 3. Parameters of the 3D decompression of an interacting Bose-Einstein condensate.

Initial radial frequency $\omega_{\perp}(0)/2\pi$	235.8 Hz
Final radial frequency $\omega_{\perp}(t_f)/2\pi$	26.2 Hz
Initial axial frequency $\omega_{\parallel}(0)/2\pi$	22.2 Hz
Final axial frequency $\omega_{\parallel}(t_f)/2\pi$	7.4 Hz
Final rescaled time τ_f	11.555 ms
Corresponding duration t_f	30.0 ms

**Figure 4.** (a) Radial and (b) axial trap frequencies for the shortcut decompression of a BEC in $t_f = 30$ ms.

Gross-Pitaevskii simulations have been performed and compared with the analytical results of Sec. 2.2. In the numerical solution we use a split step operator in time combined with a fast Fourier transformation in space. The results are presented in Fig. 5 and show that this approximation is well justified for our experimental parameters (decompression of Fig. 4, number of atoms $N \sim 10^5$, scattering length of ^{87}Rb of $a_s \sim 100 a_0$, a_0 being the Bohr radius).

3. Experimental realization of shortcuts to adiabaticity

The procedure described above was tested experimentally by quickly decompressing a trapped ultracold gas of ^{87}Rb atoms. In this section, we describe the experimental steps involved in the preparation of the cold sample (cold thermal gas or BEC) and then explain how the decompression is controlled, monitored and compared to simpler (non-optimal) schemes.

3.1. The apparatus

The Bose-Einstein condensation apparatus, sketched in Fig. 6, is formed of two chambers connected by a differential pumping tube. Each chamber is pumped by a separate ion pump. A copper tube containing solid Rubidium provides gaseous Rubidium to the upper chamber, resulting in a pressure of $\sim 10^{-9}$ mbar (100 nPa) which loads a large

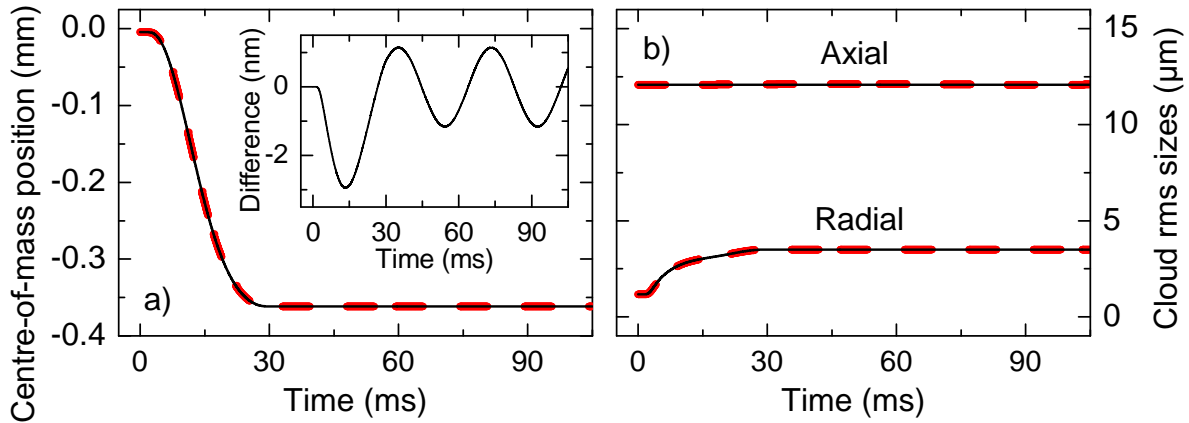


Figure 5. Comparison between the GPE simulations (dashed red lines) and the scaling solutions given by the Thomas-Fermi approximation (solid black lines) showing its validity. (a) Centre-of-mass position; (b) axial and radial sizes. The peak relative difference between the scaling solution and the GPE simulations are respectively 0.3 % and 0.2 % for the axial and radial sizes. The decompression occurs during the first 30 ms, after which the cloud evolves in the static final trap.

magneto-optical trap (MOT1). The lower chamber is a glass cell, in which a second MOT can be produced. The low-conductance tube connecting the chambers (length 10 cm, diameter 5 mm) results in a pressure on the order of 10^{-11} mbar in the second chamber. This low pressure is essential for the production of BECs because background gas collisions with the magnetically trapped atoms is the key effect limiting the efficiency of evaporative cooling.

3.1.1. Production of ultracold clouds For the production of a BEC, the first step is the loading of MOT2 from MOT1. The light of both traps is red-detuned by $\delta = -3.5 \Gamma$ from the $|5^2S_{1/2}, F = 2\rangle \rightarrow |5^2P_{3/2}, F = 3\rangle$ cooling transition of ^{87}Rb ($\Gamma/2\pi = 6.07$ MHz is the natural line width of the D_2 transition of ^{87}Rb). The six beams of both traps also contain repumper light tuned to the $|5^2S_{1/2}, F = 1\rangle \rightarrow |5^2P_{3/2}, F = 2\rangle$ transition, which prevents atoms from accumulating in the lowest energy state $|5^2S_{1/2}, F = 1\rangle$. The light is provided by two DFB diode lasers, both injected in a single-pass tapered amplifier. For both MOTs the light is delivered to the atoms by six polarization-maintaining optical fibers, to ensure a good long-term stability of the alignment. The total laser powers in MOT1 and 2 are 360 mW and 73 mW respectively, with beam waists of 2.7 cm and 6.7 mm. The magnetic field gradients of MOT1 and 2 are respectively $B'_1 = 11$ G/cm and $B'_2 = 14.6$ G/cm (these values correspond to the tighter axes).

While MOT2 is continuously on, MOT1 is operated in a pulsed regime. First, the trapping light and magnetic field are on for 100 ms and the MOT loads from the surrounding Rubidium vapour. Then, the light is switched off and a blue-detuned *pushing* laser beam, aligned on the vertical axis linking the two MOTs and passing through the differential pumping tube, is switched on for 6 ms. Because of the radiation pressure force, this light pulse transfers the atoms captured by MOT1 to MOT2 within

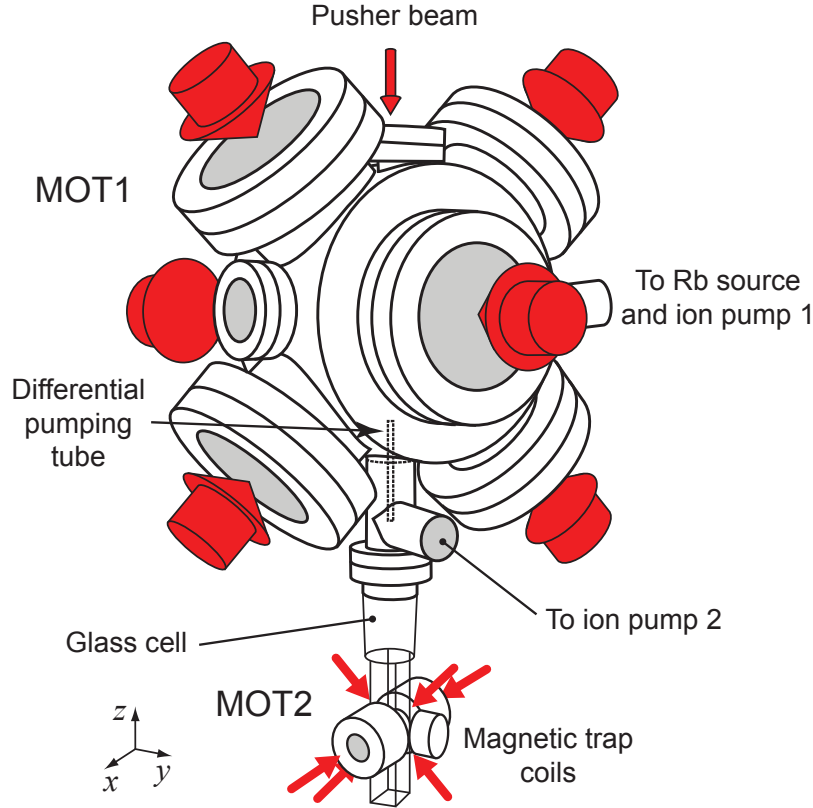


Figure 6. Schematic representation of the apparatus with the two magneto-optical trap chambers, the differential pumping tube, and the magnetic trap coils. The red arrows symbolize collimated laser beams.

15 ms. The force exerted by the pushing beam is not strong enough to overcome the trapping force of MOT2. After typically 5 to 10 seconds of such loading, MOT2 contains $\sim 10^{10}$ atoms and MOT1 is then switched off (light and magnetic field). The cloud is then compressed by a temporal dark MOT (compressed MOT): the cooling light detuning is changed from $\delta = -3.5 \Gamma$ to $\delta = -8 \Gamma$ and the magnetic field gradient is increased to $B'_2 = 65.5 \text{ G/cm}$. This reduces the multiple-scattering-induced repulsive interaction between atoms and causes the cloud to shrink, thus increasing the density and collision rate by a factor of 3. The cloud is then further cooled to $80 \mu\text{K}$ by a 3-ms-long optical molasses phase (the field is switched off, and the detuning changed to $\delta = -10 \Gamma$).

For magnetic trapping, the atoms are then optically pumped to the $|5^2S_{1/2}, F = 2, m_F = 2\rangle$ Zeeman substate by a beam detuned by $\delta_{\text{ZP}} = +3.2 \Gamma$ from the $|5^2S_{1/2}, F = 2\rangle \rightarrow |5^2P_{3/2}, F = 2\rangle$ transition and a repumper beam, detuned by $\delta_{\text{ZP rep.}} = -3 \Gamma$ is applied to the $|5^2S_{1/2}, F = 1\rangle \rightarrow |5^2P_{3/2}, F = 2\rangle$ transition. A homogeneous magnetic field of $\sim 0.5 \text{ G}$ is aligned with the light wave vector to define the quantization axis. This optical pumping stage lasts $300 \mu\text{s}$ and then, all the light is switched off and a quadrupole magnetic field (54.1 G/cm) is abruptly turned on to trap the cloud. This is

followed by an adiabatic compression of the cloud, performed by linearly increasing the magnetic gradient to 278 G/cm within 500 ms. This compression stage is primordial to increase the elastic collision rate to a high enough value, an important requirement for evaporative cooling. At this point, the number of atoms is $N \simeq 5 \times 10^9$, and the temperature $T \simeq 400 \mu\text{K}$. In order to suppress Majorana losses, the quadrupole magnetic trap is then converted into a Ioffe-Pritchard trap by adiabatically ramping the current in a third coil (quadrupole-Ioffe-configuration or QUIC trap [23]) within 500 ms. For cold enough atoms, this anisotropic trap is harmonic with radial and axial frequencies of 235.8 Hz and 22.2 Hz, respectively. Once the cloud is in the Ioffe-Pritchard trap, radio-frequency (rf) evaporative cooling is performed by ramping the rf frequency linearly from $\nu_{\text{start}} = 20$ MHz to $\nu_{\text{stop}} = 1.3$ MHz within 10 s. We are able to produce almost pure BECs (no discernible thermal fraction) containing up to 5×10^5 atoms. In order to produce an ultracold thermal cloud, the loading time of MOT2 is reduced to a few seconds. In this case, we are left, at the end of the evaporation, with a dilute, thermal gas, with a low elastic collision rate.

3.1.2. Control of the trapping frequencies Implementing shortcuts to adiabaticity requires a precise control of the trapping frequencies, in a dynamical fashion. In our QUIC magnetic trap, this can be achieved by varying the current i_Q running through the 3 coils, and the current i_{B_0} running through an additional pair of Helmholtz coils disposed along the long (axial) dimension of the trap (compensation coils). The resulting potential is

$$U(x, y, z) = \mu|\mathbf{B}| \simeq \mu \left[B_0 + \frac{1}{2} \frac{B'^2}{B_0} (x^2 + z^2) + \frac{1}{2} B'' y^2 \right] \quad (59)$$

where $\mu/h = 1.4$ MHz/G for atoms in $|5^2S_{1/2}, F = 2, m_F = 2\rangle$. B' is the radial magnetic field gradient while B'' corresponds to its curvature along y . The harmonic approximation of Eq. (59) describes accurately the potential seen by cold enough atoms i.e. $k_B T \ll \mu B_0$ [24]. Then, the radial and axial angular frequencies are

$$\omega_{\perp} \equiv \omega_z \simeq \omega_x \simeq \sqrt{\frac{\mu}{m}} \frac{B'(i_Q)}{\sqrt{B_0(i_Q, i_{B_0})}}, \quad \omega_{\parallel} \equiv \omega_y = \sqrt{\frac{\mu}{m}} \sqrt{B''(i_Q)}. \quad (60)$$

These expressions show that the radial and axial frequencies can be controlled independently to some extent. The dynamical control of the currents is achieved using homemade, computer-controlled electronic circuits. The experimental realization of shortcut trajectories requires a careful preliminary calibration of the frequencies versus currents, which is achieved by monitoring the cloud's centre-of-mass oscillations after a small excitation. Due to the finite time response of the controlling circuit, it is also necessary to check the behavior of the frequency during an actual trajectory. This is illustrated in Fig. 7, where we compare the theoretical decompression trajectory of Fig. 2 (line) and measured experimental values (circles). In this example, the deviation is below 5%.

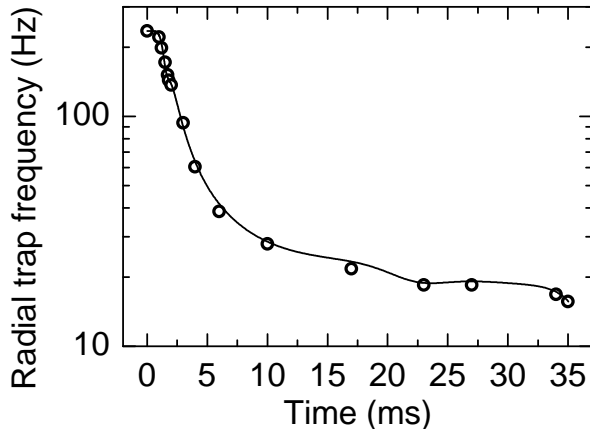


Figure 7. Vertical trap frequency calibration. The solid line is the theoretical shortcut decompression trajectory, the circles are the measured frequencies. The parameters of the decompression are given in Tab. 2.

3.2. Shortcut to adiabaticity for a non-interacting gas

For this first experiment, we use the procedure described in Sec. 3.1 to produce a thermal gas ($N \simeq 10^5$, $T_0 = 1.6 \mu\text{K}$) in the compressed trap of frequencies $\omega_x(0)/2\pi = 228.1 \text{ Hz}$, $\omega_y(0)/2\pi = 22.2 \text{ Hz}$ and $\omega_z(0)/2\pi = 235.8 \text{ Hz}$. The initial cloud-averaged collision rate per particle is $\gamma_{\text{el}} \simeq 8 \text{ Hz}$, which corresponds to a collision time of $\sim 125 \text{ ms}$. This is 30 times the oscillation period, and more than 3 times the decompression time, which justifies the non-interacting approximation.

We use here the decompression trajectory discussed in Sec. 2.1.2, adapted to the vertical axis (Oz), with the parameters of Tab. 2. To maximize the decompression factor $\gamma^2 = \omega_z(0)/\omega_z(t_f)$, the compensation coils current i_{B_0} is increased from $i_{B_0}(t=0) \simeq 0 \text{ A}$ to $i_{B_0}(t_f) = 3.0 \text{ A}$, while the QUIC current is decreased from $i_Q(t=0) = 26.7 \text{ A}$ to $i_Q(t_f) = 3.6 \text{ A}$ (see the resulting trajectory in Fig. 7). The decompression duration is $t_f = 35 \text{ ms}$.

In theory, starting from a gas at equilibrium and temperature T_0 in the compressed trap, a shortcut to adiabaticity should lead to an equilibrium state in the final trap, with a temperature $T_f = T_0 \omega(t_f)/\omega(0)$. This corresponds to a situation where entropy has not increased. On the contrary, for a non-optimal decompression, one expects to observe oscillations of the cloud's size and centre of mass in the decompressed trap, once the decompression is completed. To evaluate the efficiency of our shortcut, we thus perform the fast decompression, and hold the cloud in the decompressed trap for a variable amount of time. The trap is then abruptly switched off, and an absorption image is taken after a constant time of free expansion (6 ms). The amplitude of the dipole (oscillation of the centre of mass) and breathing modes (oscillation of the size) give access to the excess energy provided to the cloud, as compared to an adiabatic modification of the potential. If the cloud is reasonably at equilibrium after decompression, one can also directly measure the final temperature by measuring the evolution of the size during a free expansion.

In the following, we compare four decompression trajectories:

- (i) the shortcut, given on Figs. 2d and 7,

- (ii) a linear decompression of the same duration (35 ms),
- (iii) an abrupt decompression, which, somehow, corresponds to a worst case scenario (in practice, the decompression time is 0.1 ms and $\omega(t)$ is not controlled, it is imposed by the response of the magnetic trap control electronics),
- (iv) a 6-s-long linear decompression, which can be considered nearly adiabatic.

What is referred to as ‘linear decompression’ corresponds to both control currents being varied linearly with time. The corresponding frequency trajectory *is not linear*.

The experimental results are summarized on Fig. 8. In the case of the 6-s-long linear ramp (filled squares), very little residual excitation is observed (although the residual dipole mode is still measurable). In the shortcut case (open circles), clear oscillations of the cloud width and centre-of-mass position are seen, but they are much reduced compared to the fast linear ramp (diamonds) and abrupt decompression (open squares).

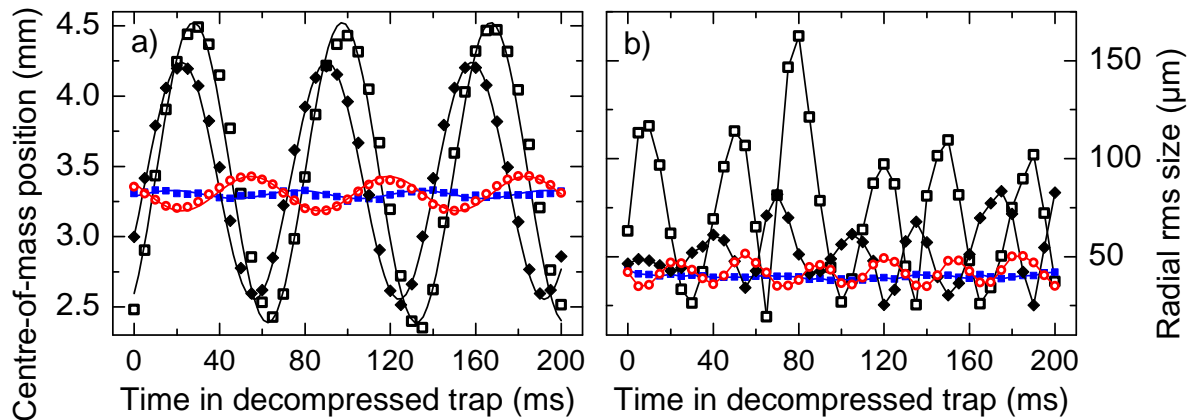


Figure 8. Comparison between different trap decompression schemes (along the vertical axis). Open red circles: shortcut decompression in 35 ms; black diamonds: linear decompression in 35 ms; solid blue squares: linear decompression in 6 s; open black squares: abrupt decompression. The decompression is performed, and then, the cloud is held in the decompressed trap for a variable time. We monitor (a) the vertical centre-of-mass position (dipole mode) and (b) the cloud size (breathing mode), after 6 ms time of flight. On (a), the solid lines are sine fits, on (b) they just connect the points to guide the eye.

Compared to the linear decompression in 35 ms, the shortcut reduces the amplitude of the dipole mode by a factor of 7.2 (obtained from the sine fits) and the amplitude of the breathing mode by a factor of 3 (comparison of the standard deviations of the two sets of data). The excess energy, which is dominated by the centre-of-mass energy, is thus reduced by a factor of ~ 52 . In the case of the 6-s-long ramp, we measured a final temperature of the cloud of 130 nK, a factor 12.5 below the initial one. This is consistent with the expected value of 15. The small difference may arise from a small heating rate due to the fluctuations of the magnetic trap.

The fact that the shortcut decompression still produces sizeable excitations is due to experimental imperfections. Several possible causes can be invoked. Firstly, as seen on Fig. 7, there are still small deviations from the ideal trajectory. These may have an impact, especially in the last phase of the trajectory where the cloud is subject to a large acceleration (see Fig. 3). Second, as can again be seen in Fig. 3, during the trajectory the cloud wanders quite far (several hundred μm) from the trap centre and feels the non-harmonic part of the potential. This effect is difficult to quantify since our knowledge of the potential shape is not sufficiently accurate (however, the anharmonicity could be inferred from variations of the oscillation frequency with amplitude). In principle, it could be avoided by designing other shortcut trajectories keeping the cloud closer to the trap centre at all times.

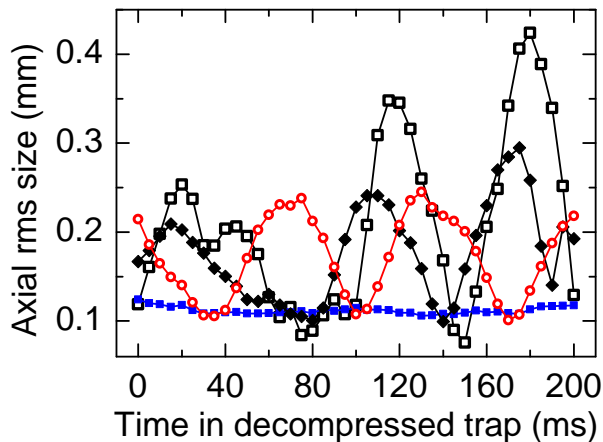


Figure 9. Impact of the vertical decompression schemes on the axial size (y direction). Same colors and symbols as in Fig. 8. The amplitude of the axial breathing mode is not affected by the use of a shortcut trajectory adapted to the radial dimensions.

Fig. 9 shows the behavior of the axial size of the cloud in the conditions of Fig. 8b. Since the shortcut trajectory was designed only for the radial dimensions, the resulting axial breathing mode is of the same magnitude as for the linear decompression.

We compare on Fig. 10 the results of the shortcut decompression to linear ramps of various durations. The vertical axis in this figure represents amplitudes of oscillations after trap decompression, either of the centre-of-mass position (filled symbols) or of the cloud radius (open symbols), scaled by their values for an abrupt decompression ($t_f \sim 0.1$ ms). The horizontal axis is the duration of the decompression t_f (notice the logarithmic scale). The circles correspond to linear decompressions while the stars are the shortcut results. As can be seen, fulfilling the adiabaticity criterion is easier for the breathing mode (size oscillation) than for the dipole mode (centre-of-mass oscillation): the oscillation amplitude is reduced by a factor of 2 for $t_f = 20$ ms for the earlier, and for $t_f \simeq 150$ ms for the latter. Using the amplitude of the dipole mode as a criterion to compare the linear and shortcut schemes, one sees that the decompression time is reduced by a factor of 37.

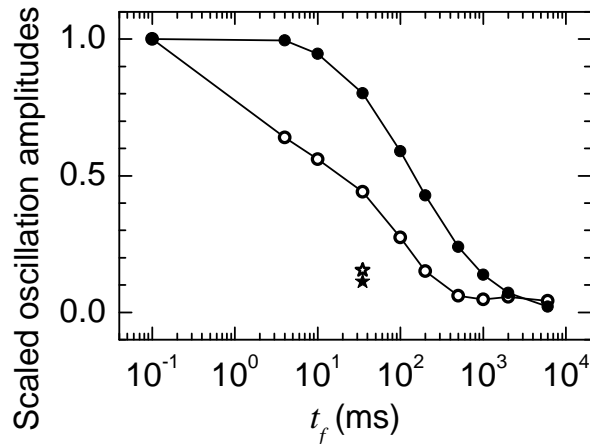


Figure 10. Comparison between linear and shortcut decompression schemes. We plot the scaled oscillation amplitudes of the breathing (cloud size, open symbols) and dipole (centre-of-mass position) modes versus the decomposition time t_f . The circles and stars correspond to linear and shortcut decompressions, respectively.

3.3. Shortcut to adiabaticity for an interacting condensate

As opposed to the previous case of non-interacting atoms, the decompression of a BEC is an intrinsically 3D problem because of the interactions. As a result, both the radial and axial frequencies have to be varied following Eqs. (56) and (57) in order to realize a shortcut to adiabaticity. In the present section, we describe a decompression experiment based on the trajectories discussed in Sec. 2.2.1 and represented in Fig. 4. In this scheme, the radial frequency is decreased by a factor of 9, while the axial frequency is adjusted to maintain the *axial size* of the BEC *fixed* during the whole trajectory. Accordingly, the axial frequency is decreased by a factor of 3.

We start from an initial BEC containing 1.3×10^5 atoms in the condensed fraction, and 7×10^4 non-condensed atoms at a temperature of 130 nK. The experimental scheme is similar to that employed for the thermal cloud. Here, we use a longer time of flight of 28 ms to characterize the various excitations generated by rapid decompressions. Three decompression schemes are compared:

- (i) the shortcut to adiabaticity in 30 ms,
- (ii) the linear decompression in 30 ms,
- (iii) an abrupt decompression.

Contrary to the previous case of a thermal cloud, the BEC cannot be held for more than 150 ms in the compressed magnetic trap because of a relatively high heating rate. Thus, here we cannot compare our scheme to the adiabatic limit corresponding to a slow linear decompression.

Figure 11 shows the temporal behaviour of the cloud following the linear and shortcut decompressions. These absorption images are taken in the (y, z) plane, after a certain holding time in the decompressed trap (indicated in the figure) plus a 28-ms-long

time of flight. The field of view is $545 \mu\text{m} \times 545 \mu\text{m}$. The centre-of-mass motion has been subtracted from these data for better clarity. In the linear case the BEC (yellow central part) experiences large deformations and oscillations of its aspect ratio, whereas in the shortcut case it remains nearly perfectly stationary. Surprisingly, in the case of the linear decompression the BEC also oscillates *angularly*. We attribute this to an uncontrolled tilt of the trap axes during the decompression. This will be discussed in more details later. The nearly isotropic aspect of the BEC after the shortcut decompression is due to the value of the time of flight, which is close to the critical time of inversion of the aspect ratio. The thermal component surrounding the BEC (red halo) is also visible. It's temporal evolution is discussed at the end of this section.

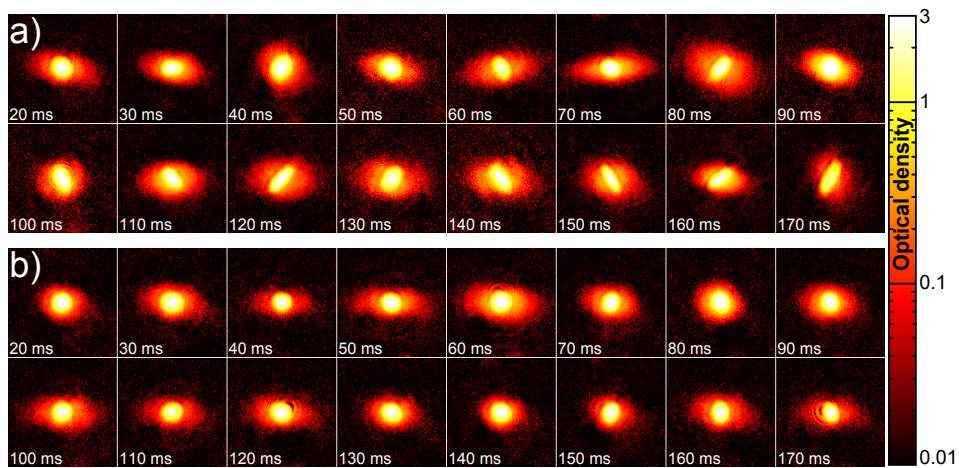


Figure 11. Comparison of linear and shortcut BEC decompressions. We compare the time evolution of the BEC after two different decompression schemes: (a) a 30-ms-long linear ramp and (b) the shortcut trajectory (see text). The centre-of-mass motion has been subtracted from these time-of-flight images for clarity. On each image, the region where the optical density is highest (yellow and white) correspond to the condensate, while the red halo is the thermal component.

To provide a more quantitative analysis, the column densities obtained from the absorption images were fitted with a 2D bimodal distribution consisting of a Gaussian component, accounting for the thermal fraction, plus a 3D inverted parabola integrated along one dimension, accounting for the condensed atoms. The fitting parameters were the cloud centre, two angles, one for each couple of eigenaxes of each components, and the two widths of each components.

In Fig. 12a) is reported the centre-of-mass oscillations (dipole mode) for the abrupt (squares), linear (diamonds) and shortcut (circles). Figure 12b) shows the oscillations of the BEC's aspect ratio (breathing mode). All measurements are performed after a 28 ms time of flight. As in the case of the non-interacting cloud, the shortcut scheme reduces the amplitude of the dipole mode compared to a standard linear decompression, here by a factor of 4.3. For our relatively long time of flight, the measured positions reflect the atomic velocities. Thus, using the shortcut scheme reduces the kinetic energy associated

with the dipole mode by a factor of 18.5 compared to the linear one (and 36 compared to the abrupt). The residual energy after the shortcut decomposition is 580 nK. As can be seen in Fig. 12b), both non-optimal schemes induce very large oscillations of the BEC's aspect ratio, with a rather complicated dynamics. A Fourier analysis reveals a main oscillation frequency of 47 Hz, consistent with a radial breathing mode at $2\omega_{\perp}$ [25–27]. A smaller contribution at 12.5 Hz corresponds to the axial breathing mode at $\sqrt{5/2}\omega_{\parallel}$ [27]. The shortcut scheme suppresses strikingly these breathing oscillations, yielding a BEC close to the targeted equilibrium state.

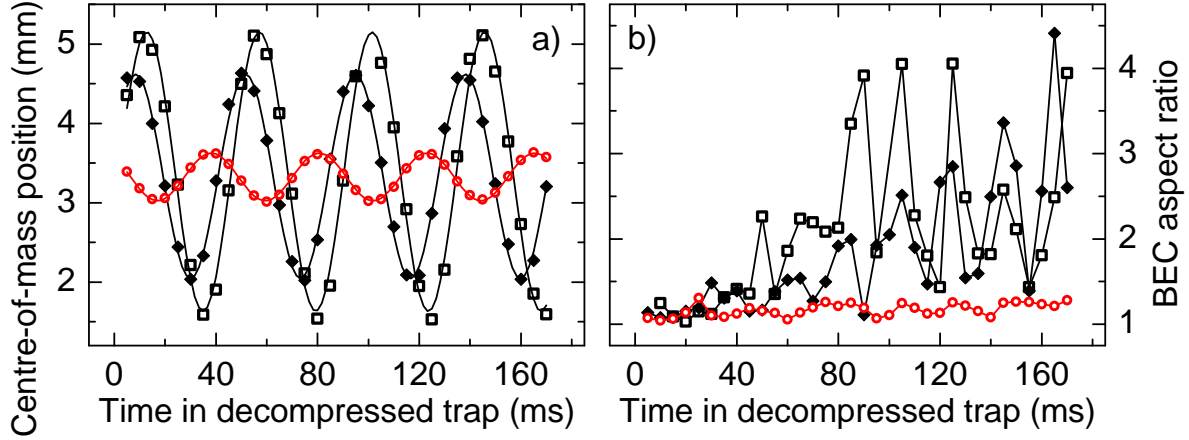


Figure 12. Decompression-induced excitations of the BEC. We report the temporal evolution of (a) the centre-of-mass position and (b) the aspect ratio of the BEC after three different decompression schemes: an abrupt decompression (black squares); a 30 ms linear ramp (black diamonds); the 30 ms shortcut trajectory (red circles). All measurements are performed after 28 ms of time of flight.

As emphasized in section 2.2, the shortcut trajectory employed in this experiment is also valid for the thermal fraction, in the radial dimensions only. This is demonstrated in Fig. 13, where we compare the oscillations of the radial (open symbols) and axial (filled symbols) sizes of a) the BEC, and b) the thermal fraction, after the shortcut decompression. The BEC's TF radius is stationary with an average value of $46.8 \mu\text{m}$ close to the theoretical value ($43 \mu\text{m}$). As can be observed in Fig. 13b), the radial size of the thermal fraction is also quite stationary as expected from a shortcut trajectory. Thus, this experiment demonstrates that both a non-interacting thermal gas and an interacting BEC can be decompressed simultaneously using an appropriate shortcut trajectory. The observed behavior is also qualitatively consistent with our initial assumption that the BEC and thermal fraction are independent. However, we expect that ultimately the validity of this approach will be limited by the interaction between the condensed and non-condensed fractions. The temperature inferred from the radial size of the thermal component is 22 nK, a factor of 6 below the initial one. This factor is smaller than the expected one ($\omega_{\perp}(0)/\omega_{\perp}(t_f) = 9$), and even if we improve the experimental set-up to realize the ideal frequency trajectory we would probably be limited by the transfer of energy from the axial breathing mode *via* the interaction with

the condensate. Indeed, the axial size of the thermal fraction presents clear breathing oscillations, reflecting the fact that the shortcut trajectory $\omega_{\parallel}(t)$ is not valid in this case, as expected.

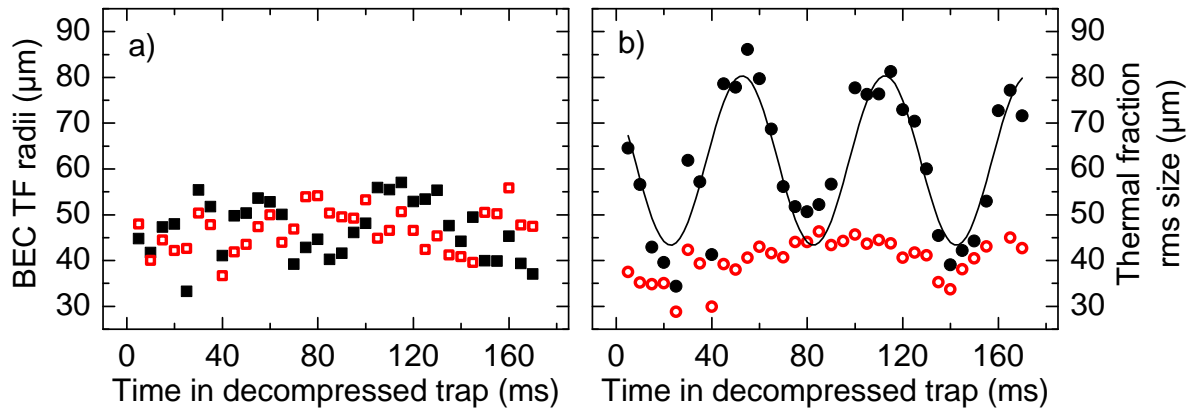


Figure 13. BEC versus thermal cloud decomposition. We plot (a) the sizes of the BEC and (b) thermal component versus the time spend in the decompressed trap for the shortcut trajectory. The filled and empty symbols correspond to the axial and radial (vertical) directions respectively. The line is a sine fit to the thermal fraction axial size.

A striking feature in Fig. 11a was the large angular oscillation of the BEC after the linear decompression. This unexpected effect is due to a slight tilt of the QUIC trap eigenaxes (3°) in the (y, z) plane as the trap centre moves downwards due to gravity. Because of this, an angular momentum is imparted to the atoms during the decompression, exciting a ‘scissors mode’ [28, 29]. Our nearly critical time of flight then results in a magnification and a deformation of the scissors oscillations [30, 31]. Fig. 14 shows an example of these oscillations, together with a GPE simulation (red line).

4. Other possible applications

In this section, we attempt to generalize the shortcut decompression of Bose-Einstein condensates to other situations which may find applications in experiments where a fast and large modification of the width of the velocity distribution or of the chemical potential is required.

4.1. Arbitrary variation of a harmonic potential

Let us consider the time evolution of a condensate in the time-dependent harmonic potential of the form

$$U(\mathbf{r}, t) = \frac{1}{2} m \mathbf{r}^t W(t) \mathbf{r} + \mathbf{r}^t \mathbf{u}(t) \quad (61)$$

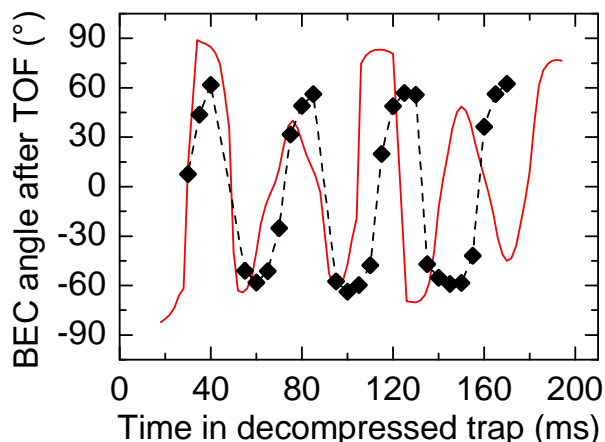


Figure 14. Experimental observation of a scissors mode excitation following the linear decompression (diamonds). The red line is a GPE simulation. The oscillation is not quantitatively reproduced because it depends on the precise way the trap is rotated during decompression, which is not known for the whole trajectory. Only the final tilt of 3° was measured. For the GPE simulation, the trap angle was assumed to be proportional to the trap bottom displacement from its original position.

where the symmetric matrix $W(t) = R^{-1}(t)\tilde{W}(t)R(t)$ represents the harmonic potential of stiffness

$$\tilde{W} = \begin{pmatrix} \omega_x^2(t) & 0 & 0 \\ 0 & \omega_y^2(t) & 0 \\ 0 & 0 & \omega_z^2(t) \end{pmatrix}, \quad (62)$$

rotated by a rotation matrix $R(t)$. The column vectors \mathbf{r} and \mathbf{u} respectively represent the position and a spatially homogeneous force which may depend on time. The superscript t indicates the transpose of vectors or matrices.

To solve Eq. (31) we look for a linear change of variables $\boldsymbol{\rho}(\mathbf{r}, \{b_{ij}(t)\}, \{r_i^{\text{cm}}(t)\})$ where the b_{ij} 's are scaling and rotation functions for the r_i 's. Let B be a 3×3 matrix which elements are the functions b_{ij} . The transformation is

$$\boldsymbol{\rho} = B^{-1}(t) (\mathbf{r} - \mathbf{r}^{\text{cm}}(t)) = B^{-1}(t)\mathbf{r} + \mathbf{a}(t). \quad (63)$$

In the TF limit, and if the matrix $\dot{B}B^{-1}$ is symmetric, Eq. (31) is invariant under this transformation. The full derivation is given in Appendix A, but we give here the key elements.

The TF approximation consists in neglecting the kinetic-energy-like term

$$\sum_{i,j,k} [B^{-1}]_{ij} [B^{-1}]_{kj} \frac{\partial^2 \chi}{\partial \rho_i \partial \rho_k}, \quad (64)$$

$\chi(\boldsymbol{\rho}, \tau)$ being defined as in Eq. (32). In this regime, the condensate wavefunction $\chi(\boldsymbol{\rho}, \tau)$ verifies the equation of motion Eq. (38), under the action of the time-independent potential

$$U(\boldsymbol{\rho}, 0) = \frac{1}{2} m \boldsymbol{\rho}^t W(0) \boldsymbol{\rho} \quad (65)$$

if the generic scaling functions satisfy

$$\ddot{B}^t B + B^t W B = \frac{W(0)}{\det B}, \quad (66)$$

$$\ddot{\mathbf{r}}^{\text{cm}} + W(t) \mathbf{r}^{\text{cm}} - \frac{1}{m} \mathbf{u} = \mathbf{0}. \quad (67)$$

It is worthwhile recalling that, as shown by the above equations, the evolution of B is decoupled from the centre-of-mass motion which evolves with the net external force. The phase of the wavefunction is chosen as

$$\phi(\mathbf{r}, t) = \frac{m}{\hbar} \left\{ \frac{1}{2} \mathbf{r}^t \dot{B} B^{-1} \mathbf{r} - \mathbf{r}^t B \dot{\mathbf{a}} \right\} + \phi_0(t), \quad (68)$$

with

$$\phi_0 = -\frac{m}{2\hbar} \int_0^t dt' \left(\dot{\mathbf{a}}^t B^t B \dot{\mathbf{a}} - \mathbf{a}^t \frac{W^0}{\det B} \mathbf{a} \right). \quad (69)$$

The wavefunction normalization is

$$\mathcal{A} = (\det B)^{-1/2}, \quad (70)$$

and the time τ is defined by

$$\frac{d\tau}{dt} = \frac{1}{\det B}. \quad (71)$$

The derivation of the scaling equations (Appendix A) relies on the particular choice of the above phase ϕ which verifies

$$\nabla_{\mathbf{r}} \phi = -\frac{m}{\hbar} B \frac{\partial \boldsymbol{\rho}}{\partial t} \quad \text{or} \quad \mathbf{v}(\mathbf{r}) = \dot{B} B^{-1} \mathbf{r} - \dot{B} B^{-1} \mathbf{r}^{\text{cm}} + B^{-1} \dot{\mathbf{r}}^{\text{cm}}, \quad (72)$$

$\mathbf{v}(\mathbf{r})$ being the velocity field of the condensate, and on the assumption that the matrix $\dot{B} B^{-1}$ is symmetric. The first condition consists in imposing that there are no terms linear in momentum in the GPE in the $\boldsymbol{\rho}$ -coordinate frame; if the first condition is fulfilled the second imposes that the velocity field is irrotational, namely that the condensate is a superfluid everywhere as well. This implies that our scaling ansatz does not take into account the presence of quantized vortices and thus can describe the dynamics of a rotated condensate only below the critical angular velocity $\dot{\alpha}_c \simeq 0.7\omega_x$ for a slightly anisotropic confinement [32], or in general, for a metastable configuration [33]. Nevertheless, a slightly modified ansatz could be devised to incorporate the possibility of quantized vortices. It is also possible to relax the first condition and allow for terms in the GPE that contain for instance the angular momentum components. These extensions are deferred for future studies.

Equations (66) and (67) can be used to determine the dipolar, compressional and scissors modes for a harmonically-trapped superfluid condensate (see Appendix B). Replacing $\det B$ with $(\det B)^\beta$ in Eq. (66), the same equation describes the compression and the scissors dynamics of a superfluid characterized by an equation of state $\mu(n) \propto n^\beta$, as it has been already shown for the quadrupolar modes [34] and as it can be easily deduced by Eq. (A.8) of the Appendix. In the following we present three possible shortcut trajectories based on these scaling equations and adapted to compress or decompress and rotate a BEC in the absence and in the presence of gravity.

4.2. Uniform decompression or compression of a condensate

We now consider the particular case of $\mathbf{u} = \mathbf{0}$ and W diagonal. If one wants to compress or decompress the condensate without modifying the condensate aspect ratio, the condition $\omega_i(t_f) = \omega_i(0)/\gamma^2$ must hold for any i . The boundary conditions for the shortcut solution are: $\dot{b}_{ii}(0) = \dot{b}_{ii}(t_f) = 0$, $b_{ii}(0) = 1$, $b_{ii}(t_f) = \gamma^{4/5}$ and $\ddot{b}_{ii}(0) = \ddot{b}_{ii}(t_f) = 0$. One possible solution is to set all $b_{ii}(t)$'s equal to a unique function

$$b(t) = \sum_{k=0}^5 c_k \left(\frac{t}{t_f}\right)^k \quad (73)$$

with $c_0 = 1$, $c_1 = c_2 = 0$, $c_3 = 10(\gamma^{4/5} - 1)$, $c_4 = -15(\gamma^{4/5} - 1)$, $c_5 = 6(\gamma^{4/5} - 1)$. The time evolution of the trap frequencies $\omega_i(t)$ will be given by the equation

$$\omega_i^2(t) = \frac{\omega_i^2(0)}{b^5} - \frac{\ddot{b}}{b}. \quad (74)$$

If the kinetic energy is negligible during the whole decompression, the final state is a BEC at equilibrium with a chemical potential that has been divided by a factor of $\gamma^{16/5}$ (because $\mu \propto (\prod_i \omega_i)^{2/5}$).

4.3. General compression or decompression in the presence of gravity

We now consider the case where $W(t)$ is diagonal with $\omega_x(t) = \omega_z(t) = \omega_\perp(t)$, $\omega_y(t) = \omega_\parallel(t)$, and $u_z = mg$. A general compression or decompression of a condensate confined in this axially-symmetric trap (51) can be realized in two steps: (i) in the first step ($t \in [0, \bar{t}]$), b_\parallel is kept fixed as outlined in Sec. 2.2, while the desired final value of $b_\perp = b_\perp(t_f)$ ($R_\perp(t_f)$) is reached; (ii) then ($t \in [\bar{t}, t_f]$) b_\perp is fixed and b_\parallel evolves according to the set of equations:

$$\omega_\perp^2(t) = \frac{\omega_\perp^2(\bar{t})}{b_\parallel(t)}, \quad (75)$$

$$\ddot{b}_\parallel(t) + b_\parallel(t)\omega_\parallel^2(t) = \frac{\omega_\parallel^2(\bar{t})}{b_\parallel^2(\bar{t})}, \quad (76)$$

$$b_\parallel(t)\ddot{c}(t) = \omega_\perp^2(\bar{t}) (c(t) - b_\parallel(t)), \quad (77)$$

where $c(t) = -\omega_\perp^2(\bar{t})r_z^{\text{cm}}(t)/(gb_\perp(t))$ as in Eq. (52). Also in this case one can write the function $c(t)$ as a polynomial of order ≥ 9 (see Eq. (50)) with the first coefficient fixed to one and the following four coefficients fixed to zero. The other coefficients are fixed by the boundary conditions at the time t_f of the function $c(t)$ and of the function $b_\parallel(t)$, that from Eq. (77) can be written as

$$b_\parallel(t) = -\frac{\omega_\perp^2(\bar{t})c(t)}{\ddot{c}(t) - \omega_\perp^2(\bar{t})}, \quad (78)$$

and by the boundary conditions of their derivatives at the same time t_f .

4.4. Rotation of the BEC in the presence of gravity

Now we propose a shortcut trajectory to rotate an axially-symmetric BEC of an angle $\bar{\alpha}$, in the presence of the gravity. In this case

$$W(0) = \begin{pmatrix} \omega_{\perp}^2(0) & 0 & 0 \\ 0 & \omega_{\parallel}^2(0) & 0 \\ 0 & 0 & \omega_{\perp}^2(0) \end{pmatrix}, \quad (79)$$

and $W(t_f) = R_{\bar{\alpha}}^{-1}W(0)R_{\bar{\alpha}}$, with

$$R_{\bar{\alpha}} = \begin{pmatrix} 1 & 0 & 0 \\ 0 & \cos \bar{\alpha} & \sin \bar{\alpha} \\ 0 & -\sin \bar{\alpha} & \cos \bar{\alpha} \end{pmatrix}. \quad (80)$$

Let us suppose, for instance, $\omega_{\perp}(0) < \omega_{\parallel}(0)$, with $\omega_{\parallel}(0) = \lambda\omega_{\perp}(0)$. The tilted ground-state for the potential $W(t_f)$ can be obtained in two steps: (i) during a time \bar{t} , fixing b_{\parallel} , decompressing the BEC in the radial direction up to the value $b_{\perp}(\bar{t}) = \lambda^{-1}$. At $t = \bar{t}$ the trap is spherical with frequency $\tilde{\omega} = \lambda\omega_{\parallel}(0)$ and the BEC is spherical with a TF radius equals to $R_{\parallel}(0)$. (ii) Fixing b_{\parallel} along the direction y' , compressing in the direction x' and z' , where the axis \mathbf{r}' are defined by $\mathbf{r}' = R_{\bar{\alpha}}\mathbf{r}$. Using the new coordinate reference frame, and setting $c_z(t) = -\tilde{\omega}^2 r_z^{\text{cm}}(t)/(gb_{\perp}(t)\cos\bar{\alpha})$, and $c_y(t) = -\tilde{\omega}^2 r_y^{\text{cm}}(t)/(g\sin\bar{\alpha})$, we obtain the set of equations

$$\ddot{b}_{\perp}(t) + b_{\perp}(t)\omega_{\perp}^2(t) = \tilde{\omega}^2/b_{\perp}^3(t), \quad (81)$$

$$\omega_{\parallel}(t) = \tilde{\omega}/b_{\perp}(t), \quad (82)$$

$$b_{\perp}^4(t)\ddot{c}_z(t) + 2b_{\perp}^3(t)\dot{b}_{\perp}(t)\dot{c}_z(t) + \tilde{\omega}^2(c_z(t) - b_{\perp}^3(t)) = 0, \quad (83)$$

$$b_{\perp}^2(t)\ddot{c}_y(t) + \tilde{\omega}^2(c_y(t) - b_{\perp}^2(t)) = 0, \quad (84)$$

the latter describing the centre-of-mass motion in the y' direction. The boundary conditions for such a problem are: $b_{\perp}(\bar{t}) = c_z(\bar{t}) = c_y(\bar{t}) = 1$, $b_{\perp}(t_f) = \lambda$, $c_z(t_f) = \lambda^3$, $c_y(t_f) = \lambda^2$, and that all the first and the second derivatives with respect to time are null at $t = \bar{t}$ and t_f . In this case a finite-order polynomial ansatz in τ for c_i was found to be inadequate as a solution of the scaling equations due to the coupling of c_y and c_z . A full numerical solution of the dynamical equation using, e.g., a shooting method [35] or following a strategy as that implemented in optimal control [9] may be needed in finding a shortcut trajectory in this case.

5. Conclusion

We have experimentally demonstrated the controlled transfer of trapped ultracold atoms between two stationary states using a faster-than-adiabatic process which reduces the transfer time down to a few tens of milliseconds. The transfer is achieved by engineering specific trajectories of the external trapping frequencies that take explicitly into account

the spatial shift introduced by gravity. This scheme was successfully applied both to a thermal gas of atoms and to an almost pure Bose-Einstein condensate. The scheme used is flexible enough to be adapted to both situations even though in the thermal gas interactions does not play a significant role while the Bose-Einstein condensate is strongly affected by the s -wave scattering of atoms. The residual excitations observed after the shortcut decompressions in the present demonstration experiments are due to our imperfect control over the time-varying magnetic trapping potential, and could be substantially reduced in future realizations.

Theoretically, the design of the transfer process was based on the invariants of motion and scaling equations techniques which turned out to be possible thanks to the harmonic shape of the external potential. In our scheme, the invariant of motion technique (for non-interacting particles) and the scaling equations technique (valid for both the non-interacting and the interacting gas) are tightly connected. The invariant of motion we used is a time-independent harmonic oscillator Hamiltonian that can be obtained by a time-dependent canonical transformation of position and momentum. In the scaling equation technique, we looked for a scaling plus shift transformation of the coordinate that allowed the equation of motion for the system to be time-independent (except for terms that are not coordinate-dependent). In both cases the whole dynamics is included in the new set of (canonical) coordinates, that depend on the trap frequencies. We also showed that these techniques can be generalized to include the rotation of the eigenaxes without much effort.

Very often, in cold-atom experiments, samples are prepared by transferring atoms from some confinement to another, e.g., from a magneto-optical trap to a magnetic quadrupolar trap, from a quadrupolar trap to a Ioffe-Pritchard trap, from an harmonic confinement to an optical lattice, etc., the main limitation being that, for short transfer times, parasitic excitations may show up. The main application of our scheme is to guide this transfer in order to prepare a very cold sample in a very short time with the desired geometry and without exciting unwanted modes. The shortcut-to-adiabacity scheme proposed here could be applied to non-interacting particles such as cold gases or ultracold spin-polarized fermions, to normal or superfluid (bosonic or fermionic as well) gases in the hydrodynamic regimes, and to strongly correlated systems such as the Tonks gas. In this paper we focused on explicit solutions to transfer atoms between two stable states, but the same strategy could be applied to control the generation of metastable states, vortex states, or some exotic out-of-equilibrium states. We plan to explore these possibilities in future studies.

Acknowledgments

This work was supported by CNRS and Université de Nice-Sophia Antipolis. We also acknowledge financial support from Région PACA, Fédération Wolfgang Doeblin, and CNRS-CONICET international cooperation grant n°22966. JFS acknowledges support from the French ministry of research and education for his funding, and thanks Mario

Gattobigio and Michel Le Bellac for helpful discussions on theoretical aspects.

Appendix A. Demonstration of Eqs. (66) and (67)

In this appendix we derive Eqs. (66)-(71). The starting point is the GPE (31) for a general potential (61). We look for a solution of the form

$$\psi(\mathbf{r}, t) = \mathcal{A}(t)\chi(\boldsymbol{\rho}, \tau)e^{i\phi(\mathbf{r}, t)} \quad (\text{A.1})$$

with

$$\boldsymbol{\rho} = B^{-1}\mathbf{r} + \mathbf{a}. \quad (\text{A.2})$$

Equation (31) then takes the form

$$\begin{aligned} & i\hbar \left[\frac{\dot{\mathcal{A}}}{\mathcal{A}}\chi + \nabla_{\boldsymbol{\rho}}\chi \cdot \frac{\partial\boldsymbol{\rho}(B, \mathbf{a})}{\partial t} + \frac{\partial\chi}{\partial\tau} \frac{\partial\tau}{\partial t} + i\chi\dot{\phi} \right] = \\ & -\frac{\hbar^2}{2m} \left\{ \sum_{i,j,k} [B^{-1}]_{ij}[B^{-1}]_{kj} \frac{\partial^2\chi}{\partial\rho_i\partial\rho_k} + 2i(B^{-1}\nabla_{\mathbf{r}}\phi) \cdot \nabla_{\boldsymbol{\rho}}\chi + i(\nabla_{\mathbf{r}}^2\phi)\chi - (\nabla_{\mathbf{r}})^2\chi \right\} \\ & + \frac{1}{2}m \{ [B(\boldsymbol{\rho} - \mathbf{a})]^t W [B(\boldsymbol{\rho} - \mathbf{a})] \} \chi + \mathbf{u}^t B(\boldsymbol{\rho} - \mathbf{a})\chi + g|\mathcal{A}|^2|\chi|^2\chi. \end{aligned} \quad (\text{A.3})$$

We look for the conditions that \mathcal{A} , B , and \mathbf{a} have to verify aiming to simplify Eq. (A.3) to the form

$$i\hbar \frac{\partial}{\partial\tau}\chi(\boldsymbol{\rho}, \tau) = \left[U(\boldsymbol{\rho}, 0) + \tilde{V}N|\chi(\boldsymbol{\rho}, \tau)|^2 \right] \chi(\boldsymbol{\rho}, \tau), \quad (\text{A.4})$$

in the TF limit, namely, neglecting the kinetic term given in Eq. (64). We deduce immediately that (i) the second term of Eq. (A.3) has to be equal to the sixth, and (ii) the first to the seventh. Condition (i) leads to

$$\nabla_{\mathbf{r}}\phi = -\frac{m}{\hbar}B \left\{ [B^{-1}]\mathbf{r} + \dot{\mathbf{a}} \right\}, \quad (\text{A.5})$$

that has a solution if the matrix $B[B^{-1}] = -\dot{B}B^{-1}$ is symmetric \ddagger . If this condition holds, we get Eq. (68) for the phase ϕ . Condition (ii) can be written as

$$\dot{\mathcal{A}}\mathcal{A}^{-1} = -\frac{1}{2}\text{tr}(\dot{B}B^{-1}). \quad (\text{A.6})$$

Using the invariance of the trace and of the determinant, the evolution of \mathcal{A} can be rewritten in term of the eigenvalues β_i ' of the matrix B as

$$\begin{aligned} \dot{\mathcal{A}}\mathcal{A}^{-1} &= -\frac{1}{2} \sum_i \frac{\dot{\beta}_i}{\beta_i} = -\frac{1}{2} \frac{\partial}{\partial t} \ln \det B \\ \frac{\partial}{\partial t} \ln \mathcal{A} &= -\frac{1}{2} \frac{\partial}{\partial t} \ln \det B \end{aligned} \quad (\text{A.7})$$

\ddagger In a general case the matrix $\dot{B}B^{-1}$ can be split into a symmetric and an antisymmetric part. In the $\boldsymbol{\rho}$ -frame of reference, the antisymmetric part gives rise to a rotational term proportional to the angular momentum and only the symmetric part of $\dot{B}B^{-1}$ contributes to the phase of the wave function. The rotational term can be neglected for nearly-isotropic trap or for small angular velocities of the trap.

If, e.g., at $t = 0$ we have that B is the identity and $\mathcal{A} = 1$, equation (A.7) yields Eq. (70).

Moreover from the comparison between the third term in Eq. (A.3) and the non-linear term (condition (iii)), we deduce Eq. (71). Taking into account (i)-(iii), Eq. (A.3) reduces to

$$\begin{aligned}
& i\hbar \frac{\partial \chi}{\partial \tau} - \hbar \det B \frac{\partial \phi_0}{\partial t} = \\
& \det B \left\{ \frac{m}{2} \left[\dot{B} B^{-1} \mathbf{r} - B \dot{\mathbf{a}}^2 + \mathbf{r}^t \ddot{B} B^{-1} \mathbf{r} + \mathbf{r}^t \dot{B} [B^{-1}] \mathbf{r} \right] \right. \\
& \left. - m \mathbf{r}^t \dot{B} \dot{\mathbf{a}} - m \mathbf{r}^t B \ddot{\mathbf{a}} + \frac{1}{2} m \left\{ [B(\boldsymbol{\rho} - \mathbf{a})]^t W [B(\boldsymbol{\rho} - \mathbf{a})] \right\} + \mathbf{u}^t B(\boldsymbol{\rho} - \mathbf{a}) \right\} \chi \\
& + g |\chi|^2 \chi.
\end{aligned} \tag{A.8}$$

By imposing the quadratic term in $\boldsymbol{\rho}$ to be equal to $\frac{m}{2} \boldsymbol{\rho}^t W^0 \boldsymbol{\rho}$, we get condition (iv), i.e., Eq. (66); the fifth condition is that the linear term in $\boldsymbol{\rho}$ vanishes and thus leads to (67); finally by requiring that the $\boldsymbol{\rho}$ -independent term be null, we get (69) for ϕ_0 .

Appendix B. Low-lying modes

Equation (67) describes the dipolar modes for the centre of mass and Eq. (66) the quadrupolar and the scissors modes. The low-lying eigenfrequencies of these latter modes can be obtained by solving the equation of motion for the matrix B for the case of a tilt of the trap of a small angle α . At $t > 0$, the matrix W is constant and can be written as

$$W = \begin{pmatrix} \omega_{\perp}^2 & 0 & 0 \\ 0 & \omega_{\parallel}^2 & \alpha(\omega_{\parallel}^2 - \omega_{\perp}^2) \\ 0 & \alpha(\omega_{\parallel}^2 - \omega_{\perp}^2) & \omega_{\perp}^2 \end{pmatrix} = W^0 + \delta W \tag{B.1}$$

where

$$W^0 = \begin{pmatrix} \omega_{\perp}^2 & 0 & 0 \\ 0 & \omega_{\parallel}^2 & 0 \\ 0 & 0 & \omega_{\perp}^2 \end{pmatrix} \tag{B.2}$$

and

$$\delta W = \begin{pmatrix} 0 & 0 & 0 \\ 0 & 0 & \alpha(\omega_{\parallel}^2 - \omega_{\perp}^2) \\ 0 & \alpha(\omega_{\parallel}^2 - \omega_{\perp}^2) & 0 \end{pmatrix}. \tag{B.3}$$

We look for solutions of the form $B^t = 1 + \delta$. Equation (66) takes the form:

$$\ddot{\delta} \simeq -W^0 \delta - \delta^t W^0 - (\text{Tr} \delta) W^0 + \delta W, \tag{B.4}$$

at the first order in δ . For the diagonal terms we have

$$\ddot{\delta}_{ii} = -2\omega_i^2 \delta_{ii} - (\text{Tr} \delta) \omega_i^2. \tag{B.5}$$

Setting $\delta_{ii} = \Delta_i e^{i\Omega t}$, we obtain the following coupled equations

$$\begin{aligned} -\Omega^2 \Delta_x &= -2\omega_\perp^2 \Delta_x - (\Delta_x + \Delta_y + \Delta_z)\omega_\perp^2 \\ -\Omega^2 \Delta_y &= -2\omega_\parallel^2 \Delta_y - (\Delta_x + \Delta_y + \Delta_z)\omega_\parallel^2 \\ -\Omega^2 \Delta_z &= -2\omega_\perp^2 \Delta_z - (\Delta_x + \Delta_y + \Delta_z)\omega_\perp^2 \end{aligned} \quad (\text{B.6})$$

whose solutions are the surface mode $\Omega = \sqrt{2}\omega_\perp$ for any values of ω_\perp and ω_\parallel , and the breathing modes $\Omega \simeq 2\omega_\perp$ and $\Omega \simeq \sqrt{5/2}\omega_\parallel$ in the cigar-shape regime $\omega_\parallel \ll \omega_\perp$.

For the off-diagonal terms δ_{ij} , ($\{i, j\} = \{2, 3\}$ or $\{3, 2\}$), Eq. (B.4) gives

$$\ddot{\delta}_{ij} = -\omega_i^2 \delta_{ij} - \omega_j^2 \delta_{ji} + \alpha(\omega_\parallel^2 - \omega_\perp^2) \quad (\text{B.7})$$

namely

$$\ddot{\delta}_{ij} + \ddot{\delta}_{ji} = -(\omega_i^2 + \omega_j^2)(\delta_{ij} + \delta_{ji}) + 2\alpha(\omega_\parallel^2 - \omega_\perp^2). \quad (\text{B.8})$$

Equation (B.8) has solution

$$\delta_{23} = \delta_{32} = \alpha \frac{(\omega_\parallel^2 - \omega_\perp^2)}{\Omega_s^2} [1 - \cos(\Omega t)], \quad (\text{B.9})$$

where $\Omega_s = (\omega_\perp^2 + \omega_\parallel^2)^{1/2}$. This is a scissors mode with boundary conditions $\dot{\delta}_{ij}(t=0) = 0$ and $\delta_{ij}(t=0) = 0$.

References

- [1] M. Born and V. Fock. Beweis des adiabatenatzes. *Zeitschrift für Physik A Hadrons and Nuclei*, 51:165–180, 1928. ISSN 0939-7922. URL <http://dx.doi.org/10.1007/BF01343193>. 10.1007/BF01343193.
- [2] Tosio Kato. On the adiabatic theorem of quantum mechanics. *Journal of the Physical Society of Japan*, 5(6):435–439, 1950. doi: 10.1143/JPSJ.5.435. URL <http://jpsj.ipap.jp/link?JPSJ/5/435/>.
- [3] Daniel Comparat. General conditions for quantum adiabatic evolution. *Phys. Rev. A*, 80(1):012106, Jul 2009. doi: 10.1103/PhysRevA.80.012106.
- [4] Claude Cohen-Tannoudji, Jacques Dupont-Roc, and Gilbert Grynberg. *Atom-Photon Interactions: Basic Processes and Applications*. Wiley, New York, 1992. ISBN 0471293369.
- [5] A. S. Parkins, P. Marte, P. Zoller, and H. J. Kimble. Synthesis of arbitrary quantum states via adiabatic transfer of Zeeman coherence. *Phys. Rev. Lett.*, 71(19):3095–3098, Nov 1993. doi: 10.1103/PhysRevLett.71.3095.
- [6] J. I. Cirac, R. Blatt, and P. Zoller. Nonclassical states of motion in a three-dimensional ion trap by adiabatic passage. *Phys. Rev. A*, 49(5):R3174–R3177, May 1994. doi: 10.1103/PhysRevA.49.R3174.

- [7] Anders S. Sørensen, Ehud Altman, Michael Gullans, J. V. Porto, Mikhail D. Lukin, and Eugene Demler. Adiabatic preparation of many-body states in optical lattices. *Phys. Rev. A*, 81(6):061603, Jun 2010. doi: 10.1103/PhysRevA.81.061603.
- [8] Xinhua Peng, Zeyang Liao, Nanyang Xu, Gan Qin, Xianyi Zhou, Dieter Suter, and Jiangfeng Du. Quantum adiabatic algorithm for factorization and its experimental implementation. *Phys. Rev. Lett.*, 101(22):220405, Nov 2008. doi: 10.1103/PhysRevLett.101.220405. URL <http://link.aps.org/doi/10.1103/PhysRevLett.101.220405>.
- [9] Ulrich Hohenester, Per Kristian Rekdal, Alfio Borzì, and Jörg Schmiedmayer. Optimal quantum control of Bose-Einstein condensates in magnetic microtraps. *Phys. Rev. A*, 75(2):023602, Feb 2007. doi: 10.1103/PhysRevA.75.023602. URL <http://link.aps.org/doi/10.1103/PhysRevA.75.023602>.
- [10] G. De Chiara, T. Calarco, M. Anderlini, S. Montangero, P. Lee, B. Brown, W. Phillips, and J. Porto. Optimal control of atom transport for quantum gates in optical lattices. *Phys. Rev. A*, 77(5):052333, May 2008. doi: 10.1103/PhysRevA.77.052333. URL <http://pra.aps.org/abstract/PRA/v77/i5/e052333>.
- [11] G. Vasilev, A. Kuhn, and N. Vitanov. Optimum pulse shapes for stimulated raman adiabatic passage. *Phys. Rev. A*, 80(1):013417, Jul 2009. doi: 10.1103/PhysRevA.80.013417. URL <http://link.aps.org/doi/10.1103/PhysRevA.80.013417>.
- [12] Michael Mundt and David J. Tannor. Optimal control of interacting particles: a multi-configuration time-dependent Hartree-Fock approach. *New Journal of Physics*, 11(10):105038, Oct 2009. doi: 10.1088/1367-2630/11/10/105038. URL <http://stacks.iop.org/1367-2630/11/i=10/a=105038>.
- [13] M. V. Berry. Transitionless quantum driving. *Journal of Physics A: Mathematical and Theoretical*, 42(36):365303, 2009. URL <http://stacks.iop.org/1751-8121/42/i=36/a=365303>.
- [14] X. Chen, A. Ruschhaupt, S. Schmidt, A. del Campo, D. Guéry-Odelin, and J. G. Muga. Fast optimal frictionless atom cooling in harmonic traps: Shortcut to adiabaticity. *Phys. Rev. Lett.*, 104(6):063002, Feb 2010. doi: 10.1103/PhysRevLett.104.063002.
- [15] H. R. Lewis, Jr. and W. B. Riesenfeld. An exact quantum theory of the time-dependent harmonic oscillator and of a charged particle in a time-dependent electromagnetic field. *Journal of Mathematical Physics*, 10(8):1458–1473, 1969. doi: 10.1063/1.1664991. URL <http://link.aip.org/link/?JMP/10/1458/1>.
- [16] Yu. Kagan, E. L. Surkov, and G. V. Shlyapnikov. Evolution of a Bose-condensed gas under variations of the confining potential. *Phys. Rev. A*, 54(3):R1753–R1756, Sep 1996. doi: 10.1103/PhysRevA.54.R1753.
- [17] Y. Castin and R. Dum. Bose-Einstein condensates in time dependent traps. *Phys. Rev. Lett.*, 77(27):5315–5319, Dec 1996. doi: 10.1103/PhysRevLett.77.5315.

- [18] Yu. Kagan, E. L. Surkov, and G. V. Shlyapnikov. Evolution of a Bose gas in anisotropic time-dependent traps. *Phys. Rev. A*, 55(1):R18–R21, Jan 1997. doi: 10.1103/PhysRevA.55.R18.
- [19] C. J. Pethick and H. Smith. *Bose-Einstein Condensation in Dilute Gases*. Cambridge University Press, 2002.
- [20] J. G. Muga, X. Chen, A. Ruschhaupt, and D. Guéry-Odelin. Frictionless dynamics of Bose-Einstein condensates under fast trap variations. *Journal of Physics B: Atomic, Molecular and Optical Physics*, 42(24):241001, 2009. URL <http://stacks.iop.org/0953-4075/42/i=24/a=241001>.
- [21] Jean-François Schaff, Xiao-Li Song, Patrizia Vignolo, and Guillaume Labeyrie. Fast optimal transition between two equilibrium states. *Phys. Rev. A*, 82(3):033430, Sep 2010. doi: 10.1103/PhysRevA.82.033430.
- [22] Jean-François Schaff, Xiao-Li Song, Pablo Capuzzi, Patrizia Vignolo, and Guillaume Labeyrie. Shortcut to adiabaticity for an interacting Bose-Einstein condensate. *Europhys. Lett.*, 93:23001, Jan 2011.
- [23] Tilman Esslinger, Immanuel Bloch, and Theodor W. Hänsch. Bose-Einstein condensation in a quadrupole-Ioffe-configuration trap. *Physical Review A*, 58(4):R2664–R2667, Oct 1998. ISSN 1050-2947. doi: 10.1103/PhysRevA.58.R2664. URL <http://link.aps.org/doi/10.1103/PhysRevA.58.R2664>.
- [24] N. R. Thomas, A. C. Wilson, and C. J. Foot. Double-well magnetic trap for Bose-Einstein condensates. *Phys. Rev. A*, 65(6):063406, Jun 2002. doi: 10.1103/PhysRevA.65.063406.
- [25] M.-O. Mewes, M. R. Andrews, N. J. van Druten, D. M. Kurn, D. S. Durfee, C. G. Townsend, and W. Ketterle. Collective excitations of a Bose-Einstein condensate in a magnetic trap. *Phys. Rev. Lett.*, 77(6):988–991, Aug 1996. doi: 10.1103/PhysRevLett.77.988.
- [26] F. Chevy, V. Bretin, P. Rosenbusch, K. W. Madison, and J. Dalibard. Transverse breathing mode of an elongated Bose-Einstein condensate. *Phys. Rev. Lett.*, 88(25):250402, Jun 2002. doi: 10.1103/PhysRevLett.88.250402.
- [27] Franco Dalfovo, Stefano Giorgini, Lev P. Pitaevskii, and Sandro Stringari. Theory of Bose-Einstein condensation in trapped gases. *Rev. Mod. Phys.*, 71(3):463–512, Apr 1999. doi: 10.1103/RevModPhys.71.463.
- [28] D. Guéry-Odelin and S. Stringari. Scissors mode and superfluidity of a trapped Bose-Einstein condensed gas. *Phys. Rev. Lett.*, 83(22):4452–4455, Nov 1999. doi: 10.1103/PhysRevLett.83.4452.
- [29] O. M. Maragò, S. A. Hopkins, J. Arlt, E. Hodby, G. Hechenblaikner, and C. J. Foot. Observation of the scissors mode and evidence for superfluidity of a trapped Bose-Einstein condensed gas. *Phys. Rev. Lett.*, 84(10):2056–2059, Mar 2000. doi: 10.1103/PhysRevLett.84.2056.

- [30] Mark Edwards, Charles W. Clark, P. Pedri, L. Pitaevskii, and S. Stringari. Consequence of superfluidity on the expansion of a rotating Bose-Einstein condensate. *Phys. Rev. Lett.*, 88(7):070405, Jan 2002. doi: 10.1103/PhysRevLett.88.070405.
- [31] M. Modugno, G. Modugno, G. Roati, C. Fort, and M. Inguscio. Scissors mode of an expanding Bose-Einstein condensate. *Phys. Rev. A*, 67(2):023608, Feb 2003. doi: 10.1103/PhysRevA.67.023608.
- [32] K. W. Madison, F. Chevy, W. Wohlleben, and J. Dalibard. Vortex formation in a stirred Bose-Einstein condensate. *Phys. Rev. Lett.*, 84(5):806–809, Jan 2000. doi: 10.1103/PhysRevLett.84.806.
- [33] A. Recati, F. Zambelli, and S. Stringari. Overcritical rotation of a trapped Bose-Einstein condensate. *Phys. Rev. Lett.*, 86(3):377–380, Jan 2001. doi: 10.1103/PhysRevLett.86.377.
- [34] Hui Hu, A. Minguzzi, Xia-Ji Liu, and M. P. Tosi. Collective modes and ballistic expansion of a Fermi gas in the BCS-BEC crossover. *Phys. Rev. Lett.*, 93(19):190403, Nov 2004. doi: 10.1103/PhysRevLett.93.190403.
- [35] William H Press, Saul A Teukolsky, William T Vetterling, and Brian P Flannery. *Numerical Recipes in Fortran 77: The Art of Scientific Computing*. Cambridge University Press, 1992. URL <http://www.nr.com>.